High magnitude and rapid incision from river capture: Rhine River, Switzerland

Brian J. Yanites,[1,2,5] Todd A. Ehlers,[2] Jens K. Becker,[3] Michael Schnellmann,[3] and Stefan Heuberger[4]

Received 25 June 2012; revised 27 February 2013; accepted 4 March 2013; published 18 June 2013.

[1] Landscape evolution is controlled by the development and organization of drainage basins. As a landscape evolves, drainage reorganization events can occur via river capture or piracy, whereby one river basin grows at the expense of another. The river downstream of a capture location will generate a transient topographic response as the added water discharge increases sediment transport and erosion efficiency. This erosional response will propagate upstream through both the captured and original river basins. Here we focus on quantifying the impact of drainage reorganization along the Rhine/Aare River system (~45,000 km^2) during the late Pliocene/early Pleistocene, where gravel remnants indicate total incision of ~650 m during the last ~4.2 Myr in the region of the recent Aare-Rhine confluence. We develop a numerical model of drainage capture to quantify the range of possible magnitudes of erosion and the transient river response resulting from the reorganization of the Rhine River. The model accounts for both fluvial incision and sediment transport. Our model estimates 400–800 m of river elevation change (lowering profiles) during the last ~4 Myr due to river capture events, providing an important component to the recent exhumation budget of the Swiss Alpine Foreland. The model indicates a rapid response to capture events (re-equilibration timescale of ~1 Myr). The predicted incision magnitudes are consistent with incision measured from the elevation of Pliocene and early Pleistocene river gravels, suggesting that across northern Switzerland, a significant amount of incision can be explained by drainage reorganization.

Citation: Yanites, B. J., T. A. Ehlers, J. K. Becker, M. Schnellmann, and S. Heuberger (2013), High magnitude and rapid incision from river capture: Rhine River, Switzerland, *J. Geophys. Res. Earth Surf.*, *118*, 1060–1084, doi:10.1002/jgrf.20056.

1. Introduction

[2] Topography results from a competition between tectonic movements that generate it and climate-driven processes that erode it. Changes in erosion rates are therefore often attributed to a change in either tectonic or climatic conditions [e.g., *Molnar and England*, 1990; *Raymo and Ruddiman*, 1992; *Whipple*, 2009]. An alternative and often less frequently considered mechanism for changing catchment erosion rates is the internal dynamics of geomorphic processes. For example, the reorganization of rivers within and amongst drainage basins (e.g., by river capture) can change catchment erosion rates by increasing the discharge and sediment flux of the river downstream of the capture location [*Bishop*, 1995]. Accelerated erosion produced by capture events generates a pulse of erosion throughout a catchment and lowers slopes to grade in equilibrium with the new discharge [*Langbein and Leopold*, 1964]. This pulse of erosion is also propagated upstream through both the captured and original river basins. Few studies have quantified the rates and magnitudes of fluvial erosion associated with river capture events [e.g., *Gunnell and Harbor*, 2010; *Schlunegger and Mosar*, 2011; *Prince et al.*, 2011; *Andrews et al.*, 2012; *Brocard et al.*, 2012], and we are not aware of studies that have explored the implications of drainage capture for landscape evolution with a numerical model.

[3] Large drainage basin reorganization events are proposed to have occurred in a number of river basins around the world including the Colorado [*Lucchitta*, 1979], Rhine [*Petit et al.*, 1996; *Ziegler and Fraefel*, 2009], Snake [*Beranek et al.*, 2006], Yellow [*Craddock et al.*, 2010], Yangtze [*Clark et al.*, 2004], Indus [*Clift and Blusztajn*, 2005], Ohio [*Gray*, 1991], and Zambezi [*Thomas and Shaw*, 1988] Rivers. Understanding the impact of drainage reorganization on erosion rates and processes is fundamental to understanding the controls on catchment denudation and landscape evolution in these regions.

Additional supporting information may be found in the online version of this article.

[1]Department of Earth and Environmental Sciences, University of Michigan, Ann Arbor, Michigan, USA.
[2]Department of Geosciences, Universität Tübingen, Tübingen, Germany.
[3]Nationale Genossenschaft für die Lagerung Radioaktiver Abfälle (Nagra), Wettingen, Switzerland.
[4]geosfer ag, St. Gallen, Switzerland.
[5]Department of Geological Sciences, University of Idaho, Moscow, Idaho, USA.

Corresponding author: B. J. Yanites, Department of Geological Sciences, University of Idaho, Moscow, ID 84844, USA. (byanites@uidaho.edu)

©2013. American Geophysical Union. All Rights Reserved.
2169-9003/13/10.1002/jgrf.20056

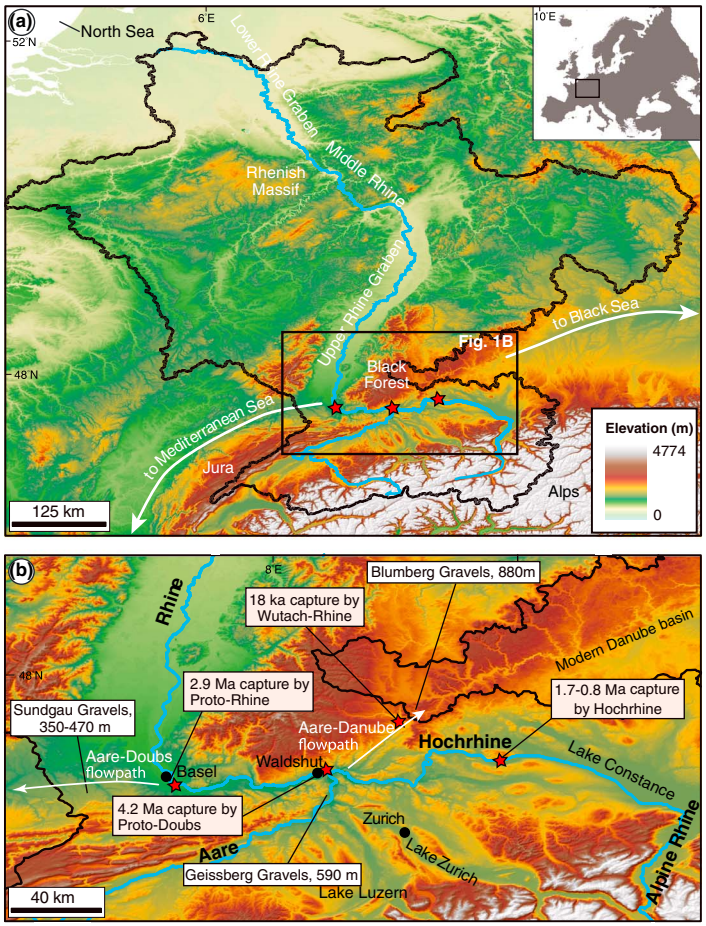

Figure 1. (a) Overview of the Rhine Basin with locations of major drainage reorganization events labeled with red stars. (b) Overview of the modern and paleo-river systems near the locations of probable drainage capture events. The towns of Basel and Waldshut are extensively referred to in the text for geographic reference. Also note the location of the Blumberg gravels relative to the modern Aare River.

[4] Here we use a simple river incision model to quantify the possible and plausible river responses to the magnitude of drainage area changes consistent with the reorganization of the Rhine River in central Europe, perhaps the best documented case of drainage reorganization in the recent geologic past (Figure 1a) [*Petit et al.*, 1996; *Berger et al.*, 2005; *Ziegler and Fraefel*, 2009; *Schlunegger and Mosar*, 2011]. Fluvial gravels along the uppermost Danube indicate that prior to ~4.2 Ma, a paleo-river flowed to the northeast from Waldshut to Blumberg (Figure 1b). This paleo-river connected the Aare and Danube River systems and drained the Swiss Alps through the Danube to the Black Sea. Following at least two drainage capture events between 4.2 and 2.9 Ma, the Aare-Rhine River was rerouted through the Upper Rhine Graben to its modern flow path (Figure 1a) [*Ziegler and Fraefel*, 2009]. The contributing drainage area upstream of Waldshut (~45,000 km^2) that formerly drained to the Danube is about one third of the modern contributing drainage area of the modern Rhine River at the North Sea. The addition of this large drainage area and discharge to its present course through the reach between Waldshut and Basel (Figure 1) and then through the Upper Rhine Graben is likely to have increased the sediment transport and bedrock erosion potential of the Rhine River. Incision caused by this event is propagated upstream through the Alpine Foreland and eventually reaches the Alps. The magnitude of the incision generated by this drainage reorganization is unknown but likely greater than 250 m [*Schlunegger and Mosar*, 2011]. Recent interest in quantifying climate and tectonic controls on erosion in the Alps and its foreland [*Kuhlemann et al.*, 2002; *Champagnac et al.*, 2007; *Norton et al.*, 2008; *Vernon et al.*, 2009; *Willett*, 2010; *Schlunegger and Mosar*, 2011] motivates a quantitative understanding of the magnitude and evolution of erosion occurring from drainage reorganization events. Understanding the controls on past erosion in the region is relevant to evaluating the impacts of future erosion on potential radioactive waste disposal sites in northern Switzerland.

[5] Here we complement previous work and quantify the spatial and temporal response of a river undergoing drainage reorganization. We use a 1-D fluvial erosion model that incorporates both sediment transport and bedrock incision to simulate the transient evolution of the Rhine River profile to a capture event. Using the constraints provided by previous geologic and geomorphic studies of the Alps, the model is calibrated to the Rhine River. Predictions from fluvial erosion models are often shrouded in uncertainty due to natural variability in model parameters. Because of

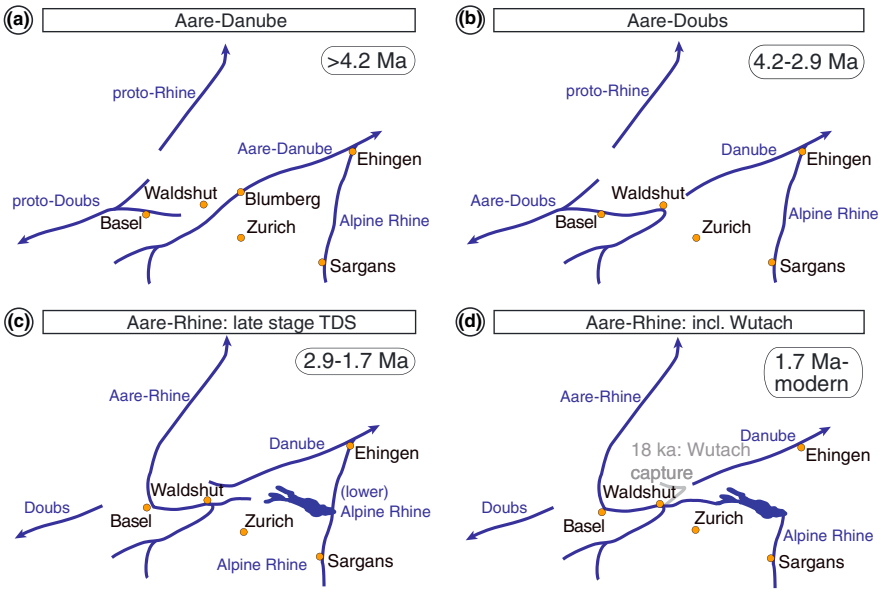

Figure 2. Schematic of drainage evolution in northern Switzerland. See text for explanation of evidence for drainage organization. (a) Aare-Danube system pre-4.2 Ma. (b) Aare-Doubs system 4.2–2.9 Ma. The Aare River is integrated into the Doubs River. (c) Aare-Rhine 2.9–1.7 Ma. The Aare is rerouted through the Upper Rhine Graben. Note that the timing for the capture of the Alpine Rhine is not precisely known (between 1.7 and 0.8 Ma; see text for further explanations). (d) Aare-Rhine, 1.7 Ma to modern. The Alpine Rhine is integrated with the Aare-Rhine system.

this, a sensitivity analysis of our "best estimate" model simulation was conducted with plausible variations in model parameters. This approach produced a wide range of possible solutions for the dynamics of Rhine catchment evolution. Finally, we discuss the implications of the results on the evolution of the topography in the Alps and Alpine Foreland, including incision magnitude and rate estimates at the Aare-Rhine confluence in the easternmost Jura Mountains (Figure 1).

[6] Although we focus on the Rhine River, the results also have implications for capture events in other regions. The model illustrates how drainage reorganization influences the dynamics of the river profile. Moreover, by modeling a range of parameter combinations, we quantify which physical parameters are important in controlling river response to drainage reorganization. Lastly, we note that the modeling framework presented in this paper can be adapted to other geographic locations where reasonable constraints on the relevant parameters can be made.

2. Geologic Background

[7] *Ziegler and Fraefel* [2009] provided a thorough review of the evolution of drainage patterns in northern Switzerland throughout the Neogene and Quaternary (~20 Ma to modern). The review covers a broad range of previous work as well as an analysis of water and wind gaps in the modern Jura that help describe more recent changes in the regional river system. They developed a series of paleogeographic maps that describe the drainage basin history in this region. We use their reconstructions to focus on major reorganization events within the Aare-Rhine system since the early Pliocene (Figure 1). Sedimentological evidence suggests that the paleo-Aare flowed toward the Danube (and eventually into the Black Sea) forming the Aare-Danube system prior to ~4.2 Ma (Figure 2a) [*Manz*, 1934; *Liniger*, 1966; *Villinger*, 1986; *Hofmann*, 1996; *Petit et al.*, 1996]. Around ~4.2 Ma, drainage reorganization diverted the Aare-Danube toward the paleo-Doubs River (and eventually into the Mediterranean Sea) forming the Aare-Doubs system (Figure 2b) [*Petit et al.*, 1996]. At ~2.9 Ma, the Aare-Doubs was captured by the Rhine River resulting in an early Aare-Rhine system draining through the Upper Rhine Graben and eventually into the North Sea (Figures 1 and 2c) [*Petit et al.*, 1996; *Hagedorn and Boenigk*, 2008]. Additionally, a portion of the Alpine Rhine remained isolated from the Aare-Doubs system and continued flowing to the Danube until the late to middle Quaternary (~1.7–0.8 Ma; Figures 1 and 2d) [*Villinger*, 1998; *Ziegler and Fraefel*, 2009; *Muttoni et al.*, 2003].

[8] Several lines of evidence support the drainage history outlined in the preceding paragraph. One example is the existence of central Alpine-derived fluvial clasts (epidote-bearing quartz gravels) located at the modern drainage divide between the Danube and Rhine basins near Blumberg [*Manz*, 1934; Figure 1]. These gravels are interpreted to be a result of the northeast flowing Aare-Danube River system. The ages of these gravels remain speculative, but they are thought to have existed since at least the early Pliocene (>4.2 Ma) [*Villinger*, 1998] and are preserved today at an elevation of ~880 m above sea level (Figures 1 and 3, Blumberg gravels), which is approximately 180 m above the modern local river elevations and ~560 m above the modern Aare-Rhine confluence near Waldshut.

[9] It is difficult to explain the existence of the Blumberg gravels without a paleo-Aare river that flowed to the northeast and into the Danube rather than turning west-northwest as it currently does. Previous interpretations of the elevation of these

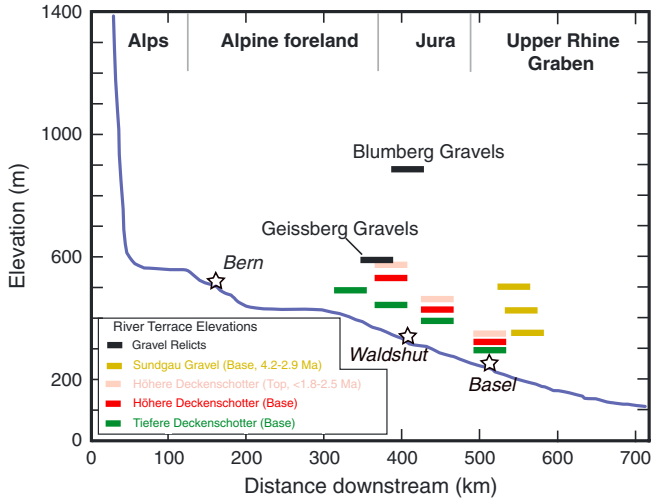

Figure 3. Plot of the longitudinal profile of the modern Aare-Rhine River (blue line) and key elevations of terraces and gravels (horizontal bars). Note the horizontal extent of the terrace bars. Locations and elevations are shown for the Blumberg, Geissberg, and Sundgau gravels as well as the Höhere and Tiefere Deckenschotter terraces. Note the Blumberg gravels are projected from their position toward Waldshut (Figure 1).

gravels were used to argue for post-depositional differential rock uplift in the Black Forest [*Müller et al.*, 2002]; however, this argument relies on assigning a correlative age to the Geissberg gravels, which are found upstream in the eastern Jura, at an elevation of ~590 m (Figures 1 and 3). The Blumberg gravels remain undated, and thus assigning a correlative age is unsupported by any geochronological data. Moreover, others have interpreted the Geissberg gravels to post-date the Aare-Danube system [*Bitterli-Dreher et al.*, 2007]. An alternative end-member interpretation would be that the rock uplift (relative to sea level) at this location is negligible, and the elevation of the Blumberg gravels denotes the pre-capture elevation of the Aare-Danube system. Such an interpretation provides an important marker for the topographic and erosional history of the Alpine Foreland and the Alps as the river basin upstream of the gravels must have been more than 880 m in elevation relative to modern sea level prior to drainage reorganization (assuming little or no rock uplift in the southeastern Black Forest). If this is the case, then we can estimate the paleo-elevation of the river upstream. The straight-line distance from the modern Aare-Hochrhine confluence to the Blumberg gravels is ~40 km. Assuming a modest slope similar to the modern Rhine of 0.0025, the paleo-Aare-Danube was ~100 m higher at Waldshut than the location of the modern Blumberg gravels (Figure 3), providing an estimate, albeit speculative, of pre-capture elevation of approximately 1000 m near Waldshut. We note that this does not include any post-deposition rock uplift of the Blumberg gravels (southeastern Black Forest) relative to Waldshut and is therefore likely a maximum, corresponding to incision of ~650 m over the last ~4.2 Myr in the region of the modern Aare-Rhine confluence.

[10] The reorganization of the Rhine from its Aare-Danube drainage configuration is supported by the arrival of Alpine-derived fluvial clasts near Basel, Switzerland (Figure 1, Sundgau gravels) at ~4.2 Ma [*Liniger*, 1966; *Petit et al.*, 1996]. Remains of these gravels can be traced along the Doubs River (at an elevation of ~200 m above the modern river) in eastern France suggesting that the reorganization of the Aare-Danube system resulted in flow into the paleo-Doubs and toward the Mediterranean (Figure 1). The elevation of these gravels relative to the modern river is variable and may be influenced by post-depositional tectonic uplift [*Giamboni et al.*, 2004; *Ustaszewski and Schmid*, 2006; *Madritsch et al.*, 2009]. These gravels are dated to the middle to late Pliocene (4.2–2.9 Ma) [*Petit et al.*, 1996].

[11] Additional evidence supporting an alternate drainage route of the Aare-Rhine system is the absence of Alpine material in the Upper Rhine Graben sediments prior to the latest Pliocene (~2.9–2.5 Ma) [*Rolf et al.*, 2008; *Hagedorn and Boenigk*, 2008]. The arrival of central Alpine clasts in the Upper Rhine Graben, noted by heavy mineral analysis, marks the establishment of the modern course of the Aare-Rhine system with headwaters beginning in the central Alps [e.g., *Liniger*, 1966; *Boenigk*, 1987; *Hagedorn*, 2004; *Hoselmann*, 2008; *Kemna*, 2008; *Weidenfeller and Knipping*, 2008].

[12] The Aare-Rhine Basin continued to grow at the expense of the Danube (including the "Alpine Rhine-Danube") throughout the Quaternary (since 2.6 Ma; Figure 3). This is evidenced by a series of gravel terrace levels, which can be mapped in the region of the modern Rhine and Aare Rivers [*Preusser et al.*, 2011]. The Höhere (higher) Deckenschotter (1.8–2.5 Ma; [*Bolliger et al.*, 1996]) and the Tiefere (lower) Deckenschotter form distinct terrace levels, which are located 100–300 m and 50–200 m above the modern river course, respectively (Figure 3). For both levels, the vertical distance between terrace level and modern river course decreases in the downstream direction. The distribution and pebble content of these Pleistocene gravels suggest that the Alpine Rhine (corresponding to the modern stretch of the Rhine upstream of Lake Constance; drainage area ~20,000 km^2), was still flowing toward the Danube after the first establishment of the North Sea-flowing Rhine [*Villinger*, 2003]. At some point during the Pleistocene, the Alpine Rhine-Danube was captured downstream of Lake Constance [*Ellwanger et al.*, 2003; *Preusser*, 2008]. It is, however, questionable whether the whole drainage area was captured at once or whether the increase in size occurred stepwise [*Ziegler and Fraefel*, 2009; *Preusser*

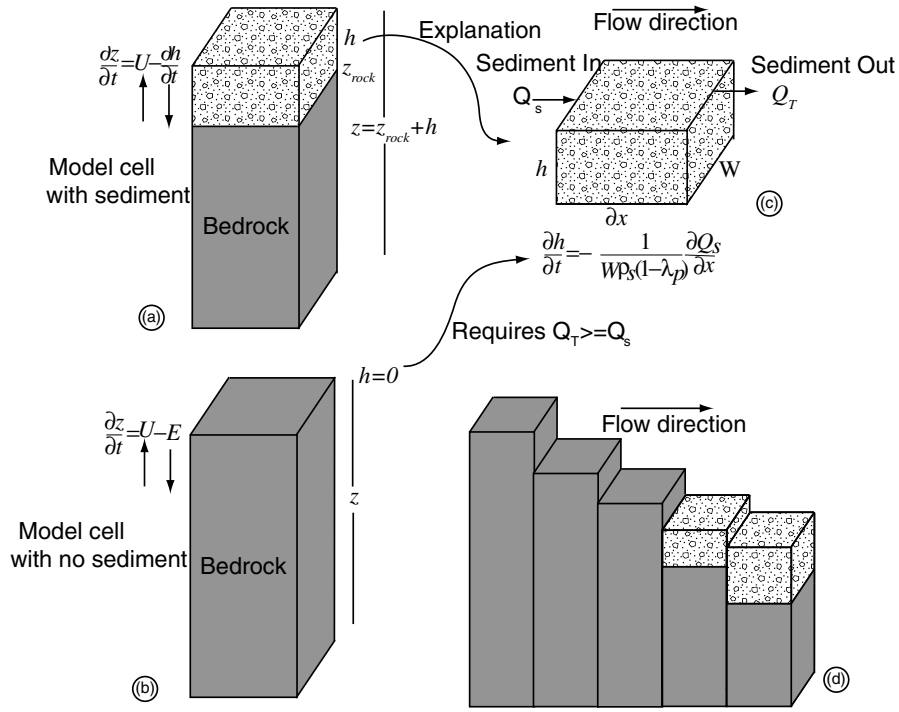

Figure 4. Model description. Elevation, z, changes based on local rock-uplift/subsidence rate and either (a) the conservation of sediment, which will deposit or remove sediment depending on the balance of sediment flux, or (b) the erosion of bedrock. In both cases, sediment fluxes are first calculated (c) to predict if the local model cell is covered by sediment (scenario A) or sediment-free (scenario B). This system of equations allows each model cell (d) to either expose bedrock for erosion or be buried in sediment depending on local conditions.

et al., 2011]. Although not as well constrained, this integration is believed to have occurred around 1.7 Ma according to *Ziegler and Fraefel* [2009]. More recently, the Wutach River captured parts of the headwaters of the Danube at ~18 ka [*Hebestreit*, 1995]. This ~200 km^2 capture event caused a wave of incision in the Wutach River. Maximum erosion rates on the order of 25 mm/yr have been inferred from late Quaternary-Holocene terrace levels [*Einsele and Ricken*, 1995]. The incision resulting from the drainage reorganization established the Wutach Gorge [*Morel et al*., 2003].

3. Methods

[13] To simulate the effects of drainage reorganization on river evolution, we developed a 1-D numerical model that incorporates both sediment transport mechanics and bedrock incision processes (Figure 4). We begin by describing the governing equations of the model that quantify changes in bed sediment thickness and bedrock elevation. Then, we describe how this model is used to model drainage capture. Next, we discuss appropriate parameter values for the Rhine River and a sensitivity analysis of these values. We then compare the predicted fluvial relief (maximum-minimum elevation) and concavity to the modern Rhine River morphology as a test of model results.

3.1. Governing Equations

[14] The elevation of the riverbed, z, over time, t, is governed by the mass balance equation:

$$\begin{aligned} \frac{\partial z}{\partial t} &= U - E \quad h = 0 \\ \frac{\partial z}{\partial t} &= U + \frac{\partial h}{\partial t} \quad h > 0 \end{aligned} \tag{1}$$

where U is the rate of rock uplift (or subsidence) relative to the geoid, E is the rate of bedrock erosion, and h is the thickness of sediment above bedrock. Bedrock erosion only occurs when sediment depth is zero (Figure 4). This allows the modeled river profile to transition from transporting sediment to eroding bedrock (or vice versa) depending on the environmental conditions.

[15] The evolution of sediment depth is governed by the Exner equation for the conservation of mass on a river bed [e.g., *Paola and Voller*, 2005]

$$\frac{\partial h}{\partial t} = -\frac{1}{W\rho_s\left(1-\lambda_p\right\}}\frac{\partial Q_s}{\partial x} \tag{2}$$

where W is the width of the channel, ρ_s is the rock density, λ_p is the sediment porosity, and Q_s is the sediment mass flux in the downstream direction, x. $\partial Q_s/\partial x$ is the divergence of bed load sediment flux in the downstream direction (sediment transported out of the reach minus sediment supplied to the reach; Figure 4).

[16] Sediment is supplied to the reach by sediment transport from the reach immediately upstream and any local sediment sources delivered by tributaries. The local material is a result of the erosion occurring in the additional drainage

area gained as the river flows downstream, ∂A. Sediment supply, Q_s, can therefore be calculated

$$Q_s = Q_O^{i-1} + \beta \rho_s E_L \partial A \tag{3}$$

where $Q_O{}^{i-1}$ denotes the magnitude of sediment transported out of the upstream reach and is calculated based on the sum (or difference) of sediment supply and material entrained/eroded (or deposited) on the bed of the upstream reach. If enough sediment is available for transport, this value will equal the transport capacity of the upstream reach. If the reach is sediment starved (i.e., transport capacity is greater than the sum of sediment supply and available bed sediment), all available sediment is transported downstream. The second term on the right side of the equation represents the amount of bed load supplied by the additional drainage area gained in the downstream direction, where E_L is the mean erosion rate in that area and β is the fraction of the eroded material in the bed load size fraction. Estimates of β along the Rhine suggest a dependence on drainage area, A [*Schlunegger and Hinderer*, 2003], which we adopt here

$$\beta = -5.06 \log A + 52.5 \tag{4}$$

where the parameters are calculated empirically.

[17] The bed load transport capacity, Q_T, of the river is calculated using an empirically derived formula [*Wong and Parker*, 2006] that depends on river shear stress, τ_b, and the median grain size, D.

$$Q_T = 3.97 \rho_s W \left[\frac{\tau_b}{(\rho_s - \rho) g D} - \tau_{c*} \right]^{3/2} D^{3/2} \sqrt{\frac{(\rho_s - \rho)}{\rho} g} \tag{5}$$

where τ_c* is the critical Shields stress, ρ is water density, and g is the gravitational acceleration constant. Note that this bed load transport formulation does not explicitly account for the hiding and protrusion effects of variable sediment size. If the sediment transport capacity is greater than the supply, Q_s, then sediment is removed from the bed (the sediment reservoir is represented by h) and added to the transported sediment mass until either the transported sediment mass equals the capacity or bed sediment thickness, h, equals zero.

[18] Shear stress is calculated using Manning's equation for a rectangular channel

$$\tau_b = \rho g \left(\frac{n Q_W}{W} \right)^{3/5} S^{7/10} \tag{6}$$

where Q_w is water discharge, S is channel slope, and n is a roughness factor, assumed equal to 0.04 for all simulations here, a value consistent for gravel bed rivers [*Chow*, 1959; *Barnes*, 1967]. Water discharge is assumed to be a function of upstream contributing drainage area

$$Q_w = k_Q A \tag{7}$$

where k_Q is an effective runoff rate to produce the average annual flood along the Rhine (see section A.1.2 for further explanation), and A the drainage area. Channel width is a function of water discharge (Q_w) and a scaling coefficient (k_w):

$$W = k_w Q_w{}^{0.5} \tag{8}$$

which is supported by empirical and theoretical studies [*Montgomery and Gran*, 2001; *Yanites and Tucker*, 2010]. For the purposes of this study, Q_w is held steady. We later discuss the implications of this assumption.

[19] If sediment depth is zero, exposed bedrock on the river bed is eroded (equation (1)). We assume a simple shear stress-dependent bedrock erosion rule

$$E = K_f \tau_b \tag{9}$$

where k_f is the bedrock erodibility and dependent on rock type and erosion process. These equations (1)–(9) are solved in an explicit, finite difference algorithm with time steps on the order of 1 year to maintain stability in the numerical solution while calculating the river profile evolution.

3.2. Model Setup for the Rhine River

[20] River profiles of the modern Aare-Rhine River were extracted from a 90 m Shuttle Radar Topography Mission digital elevation model [*Farr et al.*, 2007] to quantify distance downstream and drainage area. We also extracted the latitude and longitude of each point along the river to allow assignment of model parameters that depend on local geology, such as rock uplift or erodibility. For example, rock uplift as revealed by leveling data is a maximum in the core of the Alps and decays toward the foreland (section A.1.1) [*Gubler et al.*, 1981; *Schlatter et al.*, 2005]. Using the geography of the extracted river profile to estimate the distance from the core of the Alps, we assign values of rock uplift along the flow path of the river. This leads to the non-monotonic decline of rock uplift with distance downstream (Figure 5). We discuss a model scenario exploring spatial variations in erodibility in section 4.3.

3.2.1. Pre-Capture River Profile

[21] River capture is simulated by initially separating the river profile into two independent river profiles, one upstream (Figure 6a, red profile) and one downstream (Figure 6a, blue profile) of the capture location (Figure 6a, L_{cap}). The drainage area at the capture point on the upstream profile (Figure 6b, A_{cap}) is subtracted from all points on the downstream profile to estimate the drainage area prior to the capture event. Values of water discharge, channel width, and sediment characteristics (e.g., grain size) are then calculated based on the adjusted drainage areas (Figure 5). These pre-capture river profiles are run to steady state (i.e., erosion or sedimentation equals the rate of rock uplift or subsidence) using the equations described above to provide an initial condition for the captured river profile. Note that the final pre-capture steady state geometries are not sensitive to the initial elevations prescribed along the river. For example, starting the model with a constant elevation (plateau) or a profile that gradually slopes from 6000 m at the upstream end to sea level results in the same steady state geometry. By running these initial profiles to steady state, as opposed to a transient river system, we isolate the impacts of drainage capture on river profile evolution. After the pre-capture steady state condition is achieved, the second simulation begins and uses the pre-capture steady state geometry as the initial condition. By comparing the pre-capture geometry to the evolving, post-capture river profile, we quantify the topographic adjustment to a drainage reorganization event.

[22] In this first simulation (pre-capture), the base level of the downstream river is tied to sea-level, and the base level

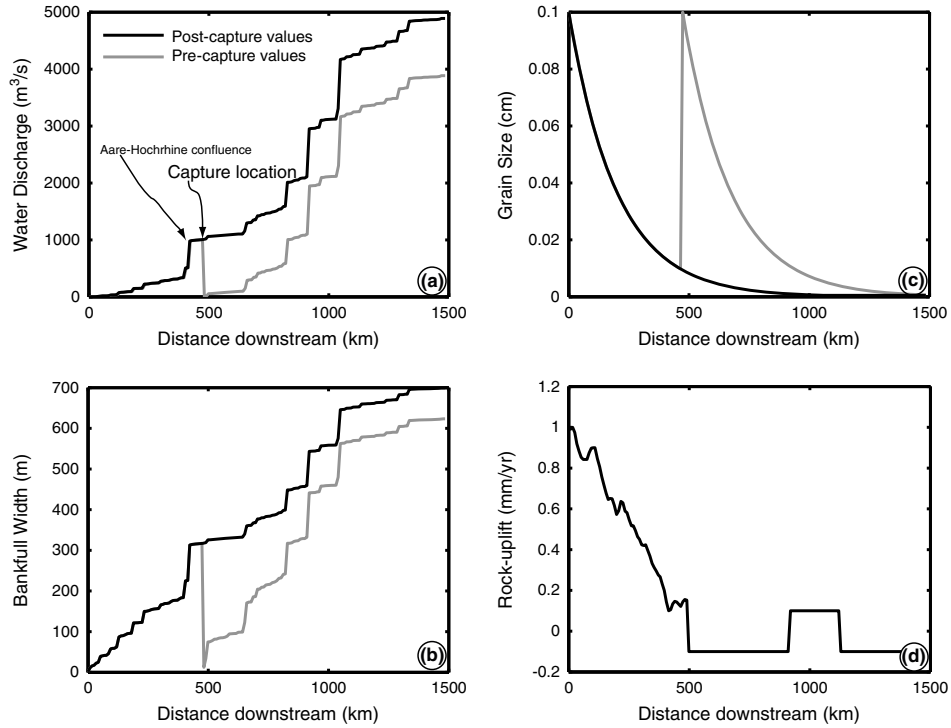

Figure 5. (a) Water discharge, (b) channel width, and (c) grain size variation with distance downstream for both pre-capture (grey) and post-capture (black) river profiles. (d) Rock uplift remains constant during pre-capture and post-capture simulations. Note that the pre-capture lines upstream of the capture point are equal to the post-capture values and are therefore hidden below the black line.

of the upstream river profile (Figure 4a, red profile) is tied to the elevation of the highest point (upstream location) on the downstream river profile (Figure 4a, blue profile). Such a geometric constraint must occur for the capture event to take place. We set the upstream location on this lower profile to be equal to a small (but not first order) drainage basin (~10 km^2) prior to the capture event. It is difficult to envision a reorganization event occurring that jumps directly to a large river without passing through any smaller tributaries, yet fluvial relief is concentrated in small drainage areas, potentially generating an unrealistically high capture elevation if the upstream location was assumed to be located on a drainage divide. Setting the drainage area to 10 km^2 accounts for both of these issues by generating a reasonable capture elevation in the baseline model (see section 4.1 below) without the need for a long horizontal distance between the two merging rivers.

[23] In our simplified setup, we model a single, large-magnitude capture event. Thereby, the downstream profile represents the river flowing through the Upper Rhine Graben and to the North Sea prior to the integration of the Aare-Rhine system. The upstream profile represents the Aare-Danube headwater stream that flowed to the modern Danube and eventually to the Black Sea, which is located ~2800km downstream of the capture location. In this model framework, the relief of the downstream profile flowing through the Upper Rhine Graben sets the elevation of the modeled capture location. An alternative approach would be to model the entire Aare-Danube system to the Black Sea; however, this would require estimates of the parameter values described above and in Table 1 for the modern Danube, which, for the most part, are less constrained than the modern Rhine. We avoid this approach as it opens up two possible issues with regard to interpreting the model results: (1) it might generate an Aare-Danube system with a lower elevation than the Upper Rhine Graben, and therefore forcing a capture to the downstream and higher profile would be nonsensical; and (2) if the modeled profile were higher than the Upper Rhine Graben river, then it would induce an additional base level signal in the incision wave. Although such a base level signal is possible, our focus is to understand the magnitude of incision because of the change in drainage area. By pinning the upstream profile to the eventual downstream profile, we ensure that the erosion signal is purely a function of drainage reorganization and not because of elevation differences.

3.2.2. Post-capture Transient Profile Adjustment

[24] At the time of capture (second simulation), the drainage area at the capture point on the upstream profile is added to all of the points on the downstream profile, and new values of water discharge, channel width, and sediment characteristics are calculated (Figure 5). Furthermore, sediment transported out of the upstream profile is added to the sediment supply of the first node on the downstream profile, effectively linking these two previously independent river systems into one river profile. The model then simulates the transient evolution of this integrated river system as it adjusts to the new environmental conditions.

[25] The development of the modern Rhine Basin has a complex history (see section 2). Given uncertainties in age constraints for the timing of capture and potential model sensitivity to parameter choices, predicting the exact erosional history with a numerical model is difficult. However, by exploring a simple scenario with only one large capture in which the modern

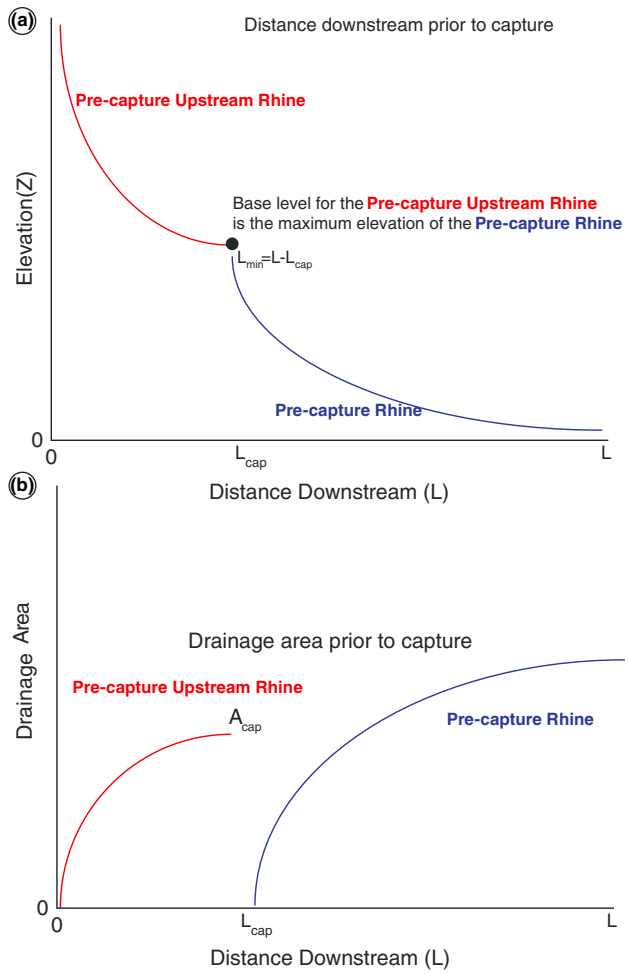

Figure 6. Schematic of the model set-up. (a) How the base level of the upstream river profile (red) is set by the assumed capture location on the downstream profile (blue). (b) The distribution of drainage area prior to capture. The values of drainage area are used to calculate water discharge, channel width, and sediment characteristics.

drainage basin upstream of Waldshut integrates through the Upper Rhine Graben provides valuable insight into two important parameters in the evolution of the Alpine Foreland.

[26] 1. It provides an estimate of river incision magnitude that can be attributed to drainage reorganization. Even if the integration occurs at different times, the cumulative incision effect of all the captures will be the same as the magnitude of all the captures occurring in a single event.

[27] 2. It provides a minimum estimate of the timescale of the transient erosional response following capture.

[28] We use this scenario as a baseline simulation. Justification of the parameterization of this baseline simulation can be found in section A and Table 1. Furthermore, from this baseline simulation, we explore model sensitivity to a number of parameters using this capture scenario to isolate the effects of parameter choices on model results. In the discussion section, we explore the implications of a more complex drainage reorganization history on landscape evolution in northern Switzerland.

3.3. Model Caveats and Sensitivity Analysis

[29] Many parameters are constrained by prior studies of the modern system (Table 1) and are used in a baseline model (see sections 4.1 below and A). The model assumes that these parameter values are constant throughout the simulation duration with the exception of the effects of drainage capture; however, this is an oversimplification. We note, however, that how these parameters varied through time along the Rhine River is not known, and therefore, model results should be viewed as estimates of plausible and probable system responses to drainage reorganization over the range of parameter space explored here. For example, glacial-interglacial climate cycles likely influence the value of water discharge over time. Knowing how a greater (or smaller) value of water discharge effects the model results helps interpret the implications of the numerical model and is the purpose of conducting a sensitivity analysis. To test the importance of parameter choices on the model results, we run a series of sensitivity analyses that are described in section 4. We test the sensitivity of model results to rock uplift, bedrock erodibility, sediment grain size characteristics, capture location, and water discharge (Table 1). The maximum/minimum values (Table 1) in the sensitivity analysis are meant to provide end-member scenarios of the model simulation to bound plausible river response scenarios to drainage reorganization in this region.

4. Results

[30] We present the baseline simulation and sensitivity analysis results, which provide rich information concerning the transience of the incision. The results are presented in Figures 6–12 and show the history of river elevation and erosion rates as a function of distance downstream. In the presentation of our results, we simplify the analysis and focus on three variables that highlight the nature of the river response: (1) the magnitude of elevation change of the riverbed at the capture point, which controls the incision magnitude that propagates upstream; (2) the maximum erosion rate; and (3) the time duration between capture and the final steady state profile, which quantifies the timescale of river adjustment. To define when a profile has reached steady state, we calculate the percent change in elevation relative to the previous model output, typically in ~50 kyr intervals. If the maximum percent change along the entire profile is less than 1%, we assume the river has achieved steady state, and we define this timescale as the "topographic adjustment" time. Choosing values smaller than 1% has little effect on the transience timescale estimate. Other important parameters, such as initial and final topographic relief, provide model validation for discerning the reliability of model results.

4.1. Baseline Model Results

[31] Figure 7 shows the model results for the parameter set based on our best estimates for the Rhine River (Table 1, baseline model). Prior to capture, the river profile is in topographic steady state (Figure 7a, upper black line), where erosion/sedimentation rate equals the rate of rock uplift/subsidence. Following capture, the river profile downstream of the capture point evolves in response to the increase in drainage area. The transient river profiles (Figure 7a, colored lines) record the profile morphology

Table 1. Model Parameters[a]

Model parameter	Description	Units	Values	Citation:
Basin/capture parameters				
L_{cap}	Capture location along the final profile	km	[370 **470** 520]	[*Ziegler and Fraefel*, 2009; and *Preusser,* 2008]
T_{cap}	Time of drainage capture before present	Ma	**4.2**	[*Ziegler and Fraefel*, 2009; and *Preusser,* 2008]
Sediment parameters				
ρ_s	Density of sediment	kg/m^3	**2650**	Assumed
β	Fraction of sediment flux as bedload	-	**Equation 4** and =0.15	[*Schlunegger and Hinderer,* 2003]
α	Sternberg exponent	1/km	**0.005**	[*Mikos*, 1994]
D_0	Headwater grain-size	cm	[20 **10** 2]	[*Mikos*, 1994]
D_{min}	Minimum bedload size	cm	**0.05**	
τ_c	Critical shields stress	-	**0.0495**	[*Wong and Parker,* 2006]
λ	Bed sediment porosity	-	**0.2**	[*Carling,* 1989]
Discharge scaling				
k_Q	$Q_w=k_Q$*Drainage area^{eQ}	m/s	[0.4 2 10]*10^{-8}	
e_Q	$Q_w=k_Q$*Drainage area^{eQ}	-	**1**	
Width scaling				
k_w	W=k_w*Drainage area^{ew}	$s^{ew}/(m^{2ew})$	**10**	
e_w	W=k_w*Drainage area^{ew}	-	**0.5**	[*cf. Yanites and Tucker*, 2010]
Other fluvial parameters				
k_f	Fluvial bedrock erodability	m^2s/kg	[10^{-4}, **10^{-5}**, 10^{-6}]	
n	Manning's n	$s/m^{1/3}$	**0.04**	
A_{crit}	Critical drainage area for channel	m^2	**10^6**	[*Montgomery and Dietrich,* 1989]

Continues

Table 1. Continued

Tectonic parameters				
Alps Rock uplift	Rock uplift rate in the Alps and Jura Mts.	mm/yr	[Uniform=0.5 mm/a; **Tilt 1 to 0.1 mm/yr**]	[*Norton et al.,* 2008; *Wittman et al.,* 2006; *Champagnac et al.,* 2007; *Kahle et al* 1997; *Gubler et al* 1981; *Schlatter* et al., 2004]
Upper Rhine Graben subsidence	Subsidence in the Upper Rhine Graben	mm/yr	[**-0.1 mm/yr**; -0.01 mm/yr]	[*Hagerdorn and Boenigk,* 2008]
Rhine Massif Rock uplift	Middle Rhine (Rhine Massif) rock uplift rate	mm/yr	**.1 mm/yr**	[*Boenigk and Frechen*, 2006]
Lower Rhine Graben subsidence	Lower Rhine subsidence	mm/yr	**-0.1 mm/yr**	[*Zagwijn,* 1989]
Additional sediment supply parameters				
Sediment supply rate (per m^2) from tributaries to Upper Rhine Graben		mm/yr	**0.05 mm/yr**	
Sediment supply rate (per m^2) from tributaries to Lower Rhine Graben		mm/yr	**0.005 mm/yr**	
Constants				
ρ_w	density of water	kg/m^3	**1000**	Archimedes
g	gravitational acceleration	m/s^2	**9.8**	Galileo Galilei and Sir Isaac Newton
			baseline model	sensitivity analysis

[a]Grey boxes represent sensitivity analysis. Baseline model values are bold.

every ~67 kyr (15 profiles) following the capture until the river reaches a new steady state at ~1 Myr. This baseline model results in an ~725 m elevation change immediately upstream of the capture point due to drainage reorganization (Table 2 and Figure 6a). This additional incision is beyond the erosion necessary to maintain topographic steady state. For example, a reach of river that experiences 0.3 mm/yr of rock uplift would have eroded ~1025 m of material over the 1 Myr of profile adjustment (725 m from the capture, 300 m from maintaining steady state).

[32] The difference between the pre-capture and post-capture river profiles decays downstream of the capture point to where no elevation change occurs at ~650 km downstream (Figure 7a). Between ~650 and 1000 km, a slight (<40 m) gain in elevation occurs by a rapid (<130 kyr) transient increase in the rate of sediment aggradation in the Upper Rhine

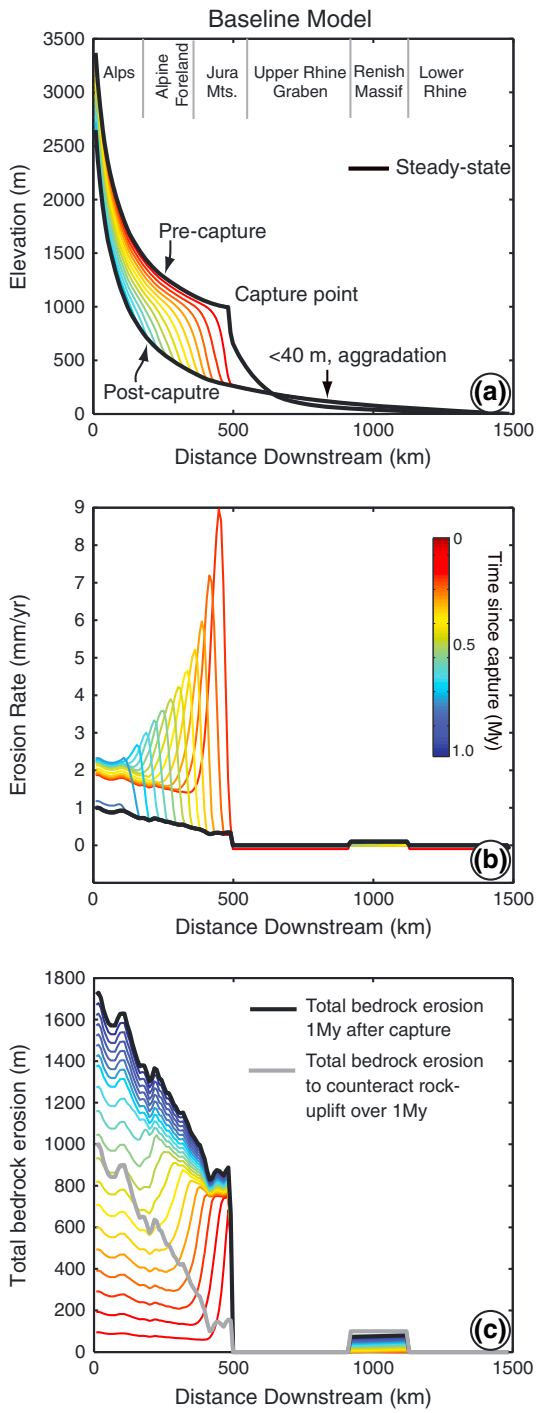

Figure 7. Baseline model results. (a) The evolution of the river profile following capture. Color of line denotes its age in 67 kyr increments. Bold black lines are the pre-capture and post-capture steady state profiles. (b) The evolution of erosion rate. Note peak erosion occurs just after capture and decays as the signal propagates upstream. (c) Total bedrock erosion since time of capture. Erosion at ~1000 km is from uplift of the Rhenish Massif [*Boenigk and Frechen*, 2006]. Note that remobilization of deposited sediment is ignored resulting in the sharp break at the Upper Rhine Graben. Grey line represents the bedrock erosion over 1 Ma for a system in steady state with the imposed rate of rock uplift.

Graben. Downstream of ~1000 km, the two profiles are nearly indistinguishable.

[33] Figure 7b shows the evolution of erosion rates along the river for 15 time slices (0–1 Myr following capture) while the profile responds to the transience of the drainage reorganization. Upstream of the capture point, erosion rate increases everywhere almost instantaneously with a maximum at the capture point. The maximum erosion rate of ~11 mm/yr occurs just downstream of the capture point and immediately following the capture event (note that due to regularly spaced time slices, the maximum erosion rate may not be shown in the figure). It should be noted that this peak erosion, although large, is short lived and quickly decays as shown by subsequent lines. The peak erosion migrates upstream as the transience propagates through the Rhine River. This pattern of erosional response (i.e., a migrating knickpoint superimposed on uniform increase in erosion rate) is a result of the combination of sediment transport and detachment-limited erosion fluvial models [*Whipple and Tucker*, 2002].

[34] In Figure 7c, we plot the total bedrock erosion magnitude along the profile following the time of capture. This value is the time-integrated erosion (different times, again, are denoted by different colors) and shows how much bedrock material has been removed since capture. Note that in this plot, the erosion of previously deposited river sediments (i.e., in the Upper Rhine Graben) is ignored to focus only on bedrock erosion. This results in the sharp break in the plot at the start of the Upper Rhine Graben (~500 km) where bedrock is located well below sea level due to long-term subsidence. We plot the total bedrock erosion that occurs over 1 Myr following basin integration in black (Figure 7c). In grey, the magnitude of erosion expected to maintain topographic steady state over 1 Myr is plotted (i.e., the integral of rock uplift). The difference between the black and grey lines is the elevation change due to river capture along the river profile. This plot highlights the additional erosion occurring along the Rhine River due to the basin reorganization.

4.2. Sensitivity of Results to Rock Uplift/Subsidence Patterns

[35] Two simulations were conducted to test the influence of our rock uplift pattern on model results. First, we changed rock uplift to a uniform value of 0.5 mm/yr upstream of the Upper Rhine Graben. The evolution of the profile (Figure 8a) showed little difference in comparison to the baseline model. As in Figure 7, the pre-capture and post-capture steady state fluvial profiles are shown in black with transient profiles in color (Figure 8a). Furthermore, neither the maximum erosion rate (Figure 8b and Table 2) nor the timescale of adjustment (Table 2) changed dramatically compared to the baseline model. In the second simulation, the rate of subsidence in the Upper Rhine Graben was lowered by an order of magnitude (Table 1). This results in a very similar transience of the profile compared to the baseline model (Table 2 and Figures 7c and 7d). The elevation difference between the headwaters and mouth of the river (i.e., fluvial relief) is also minimally affected in both scenarios (Figures 7a and 7c).

4.3. Sensitivity of Results to Bedrock Erodibility

[36] Four simulations were conducted to test the sensitivity of river profile evolution to variations in the lithologic resistance to erosion, the erodibility parameter.

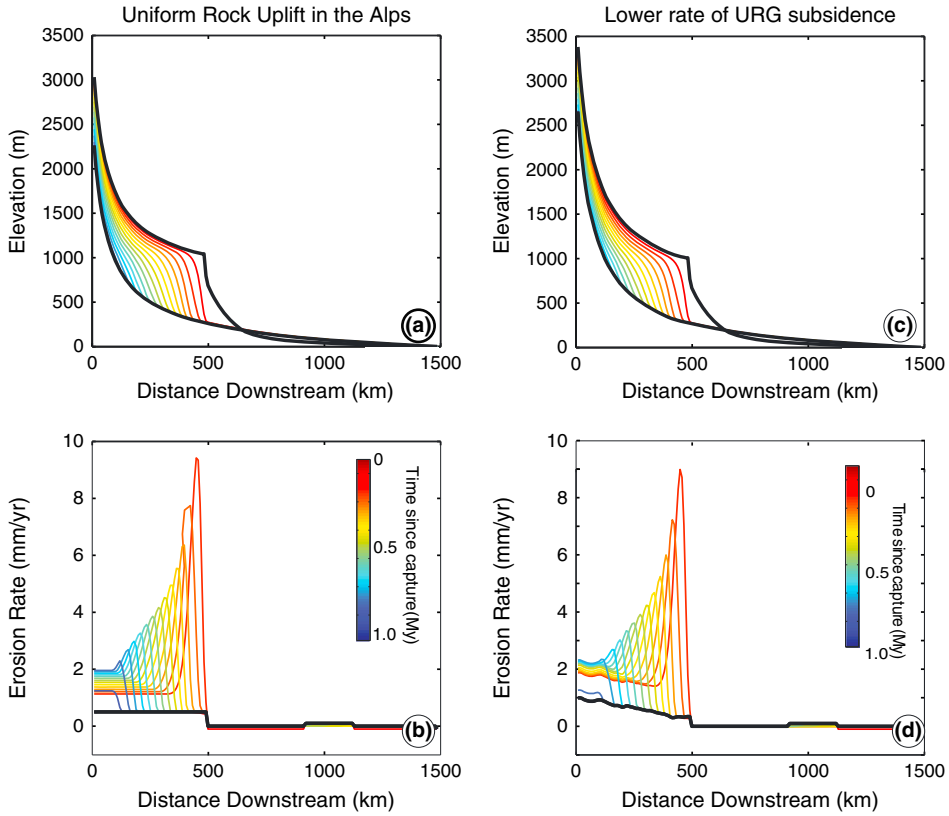

Figure 8. Model sensitivity to rock uplift and subsidence. (a and c) The evolution of the river profile following capture. Color of line denotes its age. Bold black lines are the pre-capture and post-capture steady state profiles. (b and d) The evolution of erosion rate. Note the similarities in both systems to Figure 7.

The erodibility was increased (i.e., a more easily eroded material) for two simulations (10^{-3} and 10^{-4} m^2 s/kg) and decreased for one simulation (10^{-6} m^2 s/kg). These values are chosen to represent a potential range of lithologies from poorly indurated sedimentary rock to hard, unfractured crystalline bedrock. Such a broad range was explored because erodibility is a poorly quantified parameter for natural systems (see section A.1.2). Results from previous studies suggest that erodibility values for the lithologies present in our study area (granite, moderately lithified sediments) have erodibilities that cover the same range of values used in this study [*Stock and Montgomery*, 1999; *Yanites et al.*, 2010]. Few other studies of calibrated river incision models exist to date, and we therefore use the results of *Yanites et al.* [2010] to guide our parameter choice. The fourth simulation tested the influence of spatial variations in lithology where erodibility was varied from 10^{-6} m^2 s/kg in the Alpine highlands to 10^{-4} m^2 s/kg at the foot of the Jura Mountains. The impact of bedrock erodibility on the incision magnitude, maximum erosion rate, and timescale of adjustment on river evolution is variable. Increasing bedrock erodibility has little effect on incision magnitude (Table 2 and Figures 8a and 8c), but a strong influence on maximum incision rate (Figures 9b and 9d) and the timescale of adjustment (Table 2). The maximum incision rate increases to >100 mm/yr for an order of magnitude increase in erodibility and to >500 mm/yr for an increase of 2 orders of magnitude above the baseline simulation. Both scenarios with higher erodibility adjusted to a new steady state profile in less than 50 kyr.

[37] Decreasing bedrock erodibility has a relatively small effect on incision magnitude (Figure 9e) compared to the baseline model. The maximum elevation change is ~975 m (~34% higher than the baseline). The maximum rate of incision of ~2.3 mm/yr is significantly lower than the baseline model. The timescale for topographic adjustment is much longer (>10 Myr) than any other simulation tested in this study. We note that decreasing erodibility results in unrealistically high fluvial relief (18 km, note the y axis scale in Figure 9e) highlighting that this value clearly represents an unrealistic lower end-member for fluvial erodibility in the region.

[38] Variations in lithology with successively higher erodibility in the foreland compared to the Alps have little influence on either the magnitude of incision or the timescale of adjustment (Table 2 and Figure 9g). The maximum incision rate, on the other hand, is twice the rate of the baseline model (Figure 9h). This suggests a strong spatial variability in the response, where near the capture point, the profile adjusts much more quickly in this variable lithology model than the baseline model. The relief of the profile is sensitive to the pattern of bedrock erodibility. By incorporating rocks that are less erodible in the headwaters, relief along the profile increases by ~1500 m even though more erodible rocks are present than the baseline simulation. This occurs because at high erodibility ("soft" rocks), the slope of the river is strongly influenced by imposed sediment loads, and thus the river slope is strongly influenced by the sediment transport capacity. Because the imposed sediment load is the same between these simulations, a change to even

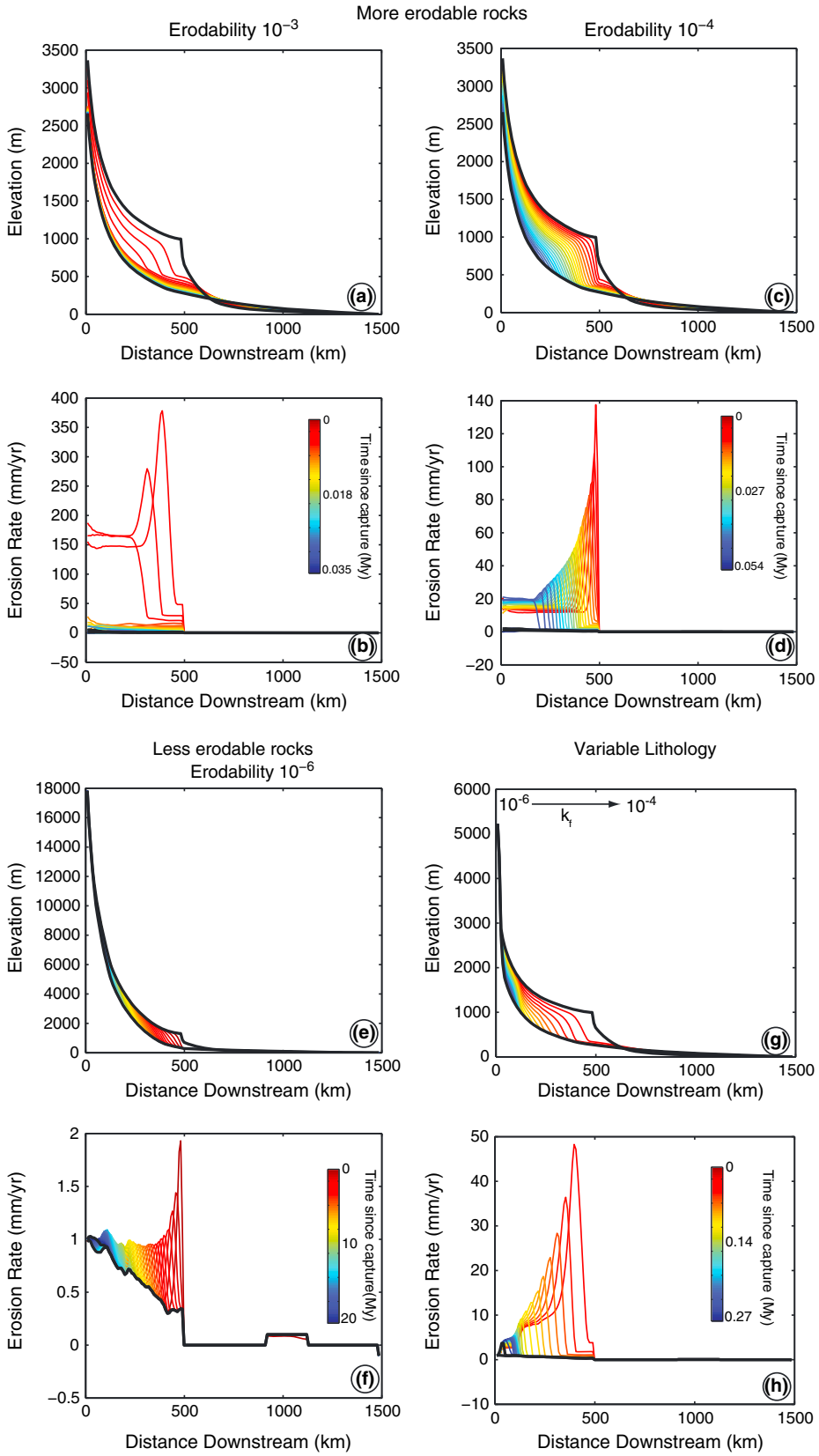

Figure 9. Results for the sensitivity analysis of bedrock erodibility. (a, c, e, and g) The evolution of the river profile following capture. Color of line denotes its age. Bold black lines are the pre-capture and post-capture steady state profiles. (b, d, f, and h) The evolution of erosion rate. Note the *y* axis scale varies in the subplots.

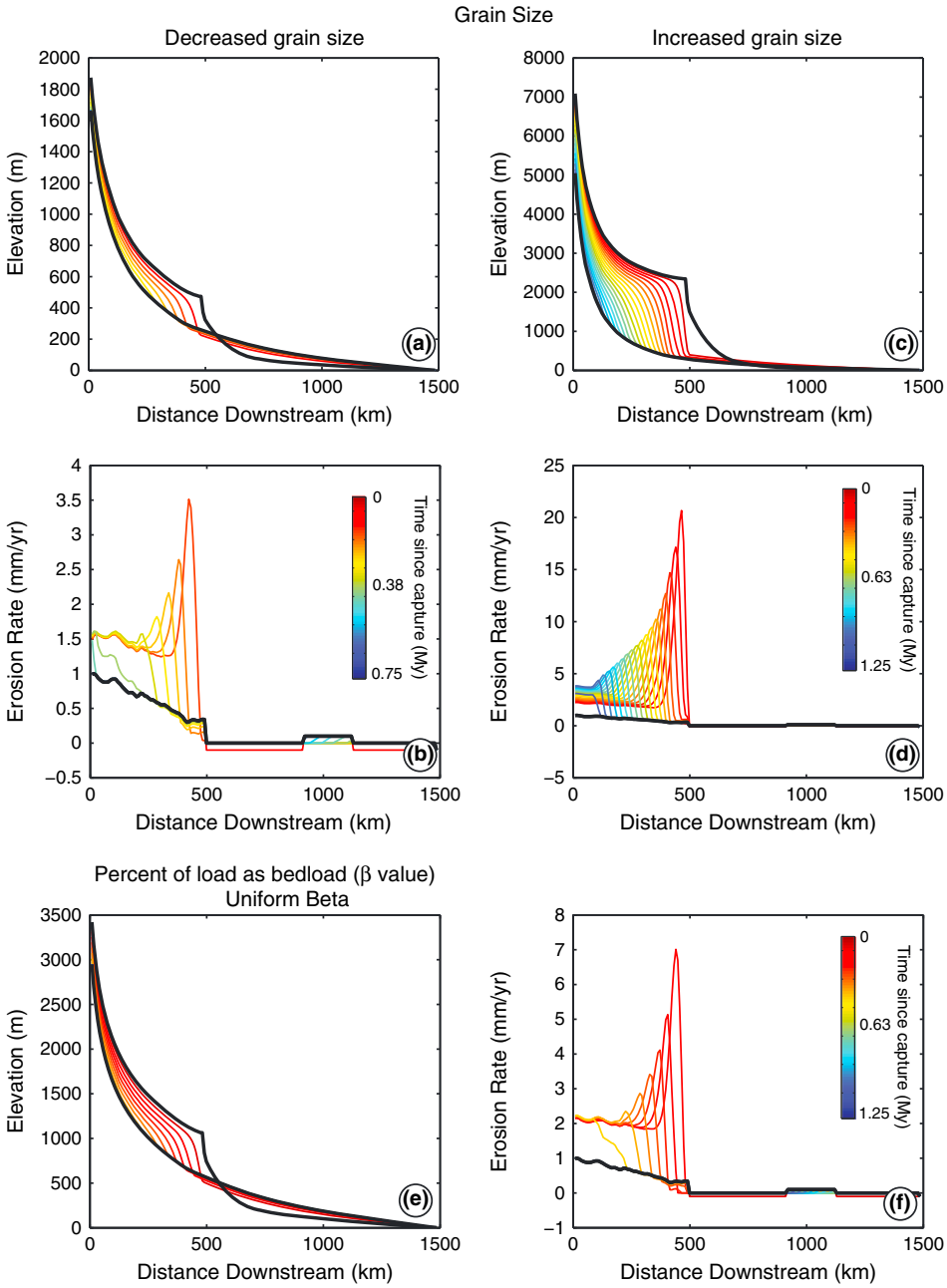

Figure 10. Model sensitivity to sediment characteristics. The evolution of the river profile following capture for (a) smaller and (c) greater grain sizes. (e) The sensitivity to the pattern of the percentage of material transported by bed load. Color of line denotes model time following transience. Bold black lines are the pre-capture and post-capture steady state profiles. (b, d, and f) The evolution of erosion rate. Note the similarities in both systems to Figure 7. Note the *y* axis scale varies in the subplots.

higher erodibility has little effect on slope. This results in a greater sensitivity to less erodible rocks ("hard" rocks; Figures 9e and 9f) than more erodible rocks ("soft" rocks; Figures 9a–9d) compared to the baseline model.

4.4. Sensitivity of Results to Sediment Grain Size Characteristics

[39] Three simulations were conducted to test the model sensitivity to grain size. Two simulations investigated the initial grain size assumed in the river headwaters. The first reduced the grain size by half compared to the baseline model (10 cm median grain size in the headwaters), whereas the second doubled the initial grain size. The third simulation tested the assumption that the percent of sediment load transported by bed load varies downstream [*Schlunegger and Hinderer*, 2003] by assuming a uniform bed load fraction. Model results all showed a strong sensitivity to grain size (Table 2 and Figure 9). Decreasing the headwaters median grain size by half reduces the magnitude of incision to 214 m (a reduction of ~70%), whereas doubling the median grain to 20 cm increases the magnitude of incision to >2000 m. This produces unrealistic relief (Figure 9C).

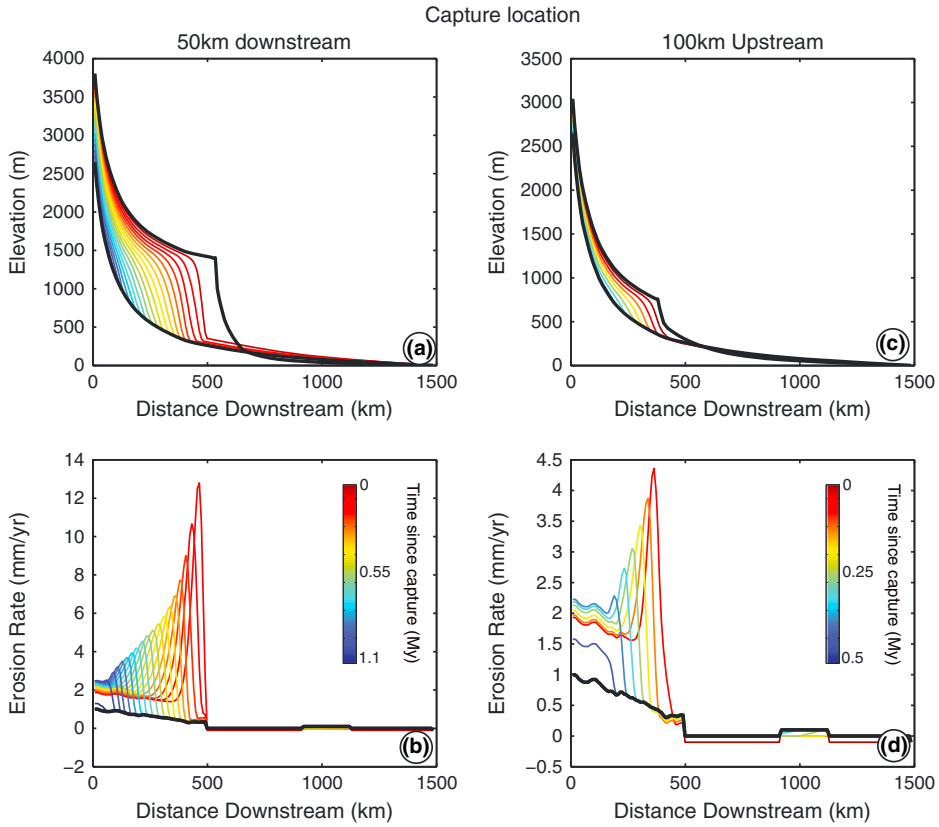

Figure 11. Model sensitivity to capture location. The evolution of the river profile following capture for a capture event located (a) 50 km downstream of the baseline model and (c) 100 km upstream of the baseline model. Color of line denotes its age. Bold black lines are the pre-capture and post-capture steady state profiles. (b and d) The evolution of erosion rate. Note the *y* axis scale varies in the subplots.

Further, more than 2 km of erosion in northern Switzerland is unlikely as terrace records suggest much less incision [e.g., *Preusser et al*., 2011]. Maximum incision rates and transience timescale are also sensitive to grain size, though the sensitivity is less than incision magnitude. For example, with a decrease in grain size (Figures 10a and 10b), the maximum incision rate is lowered to ~5 mm/yr, and the profile responds in less than 500 kyr. For an increase in grain size, maximum incision reaches >20 mm/yr with a profile response timescale of ~1 Myr.

[40] Assuming a uniform distribution of the proportion of bed load material (e.g., no downstream dependence of β), predicts only ~480 m of incision (Table 2 and Figure 9e) but the maximum incision rate of 9.5 mm/yr is similar to the baseline model (Table 2 and Figure 10f). The timescale of response suggests a slightly more rapid equilibration (<500 kyr) if bed load proportion is constant along the river profile. This scenario is likely an unrealistic end-member case due to the tendency for a reduction in grain size in the downstream direction.

4.5. Sensitivity of Results to Capture Location

[41] The position of the capture point is not precisely known, which requires an analysis of our assumed capture location. Locating the capture point 50 km downstream of the baseline model increases all three profile response parameters (Table 2). The magnitude of incision increases to >1100 m (Figure 11a), the maximum incision rate increases to ~16 mm/yr (Figure 11b), and the timescale of response increases to ~1 Myr (Table 2). Moving the capture location 100 km upstream decreases all three parameters. The magnitude of incision decreases to ~400 m (Figure 11c), the maximum erosion rate decreases to ~4.9 mm/yr (Figure 11d), and the profile responds in <500 kyr (Table 2).

[42] The slope of a river in a subsiding reach is highly sensitive to the interplay between grain size, sediment supply, and water discharge [*Paola et al*., 1992, and *Sinha and Parker*, 1996]. Moreover, the proportion of bed load (equation (4)) and grain size both depend on drainage area; therefore, the distribution of sediment characteristics along the Rhine River is controlled by the network geometry of the drainage basin. Because of how subsidence, the drainage network, and sediment characteristics vary near the boundary of the Upper Rhine Graben, different pre-capture relief scenarios are generated for the different modeled capture locations. This leads to the different model results found in this analysis. In other words, for river reaches near the headwaters, the increase in drainage area with distance downstream occurs more slowly in the downstream capture location case than in the upstream case. This causes steeper slopes over a longer horizontal distance, resulting in more relief in the headwaters.

4.6. Sensitivity of Results to Variations in Discharge

[43] In addition to capture events, water discharge can also vary in response to climate change, which has undoubtedly occurred throughout the evolution of the Rhine

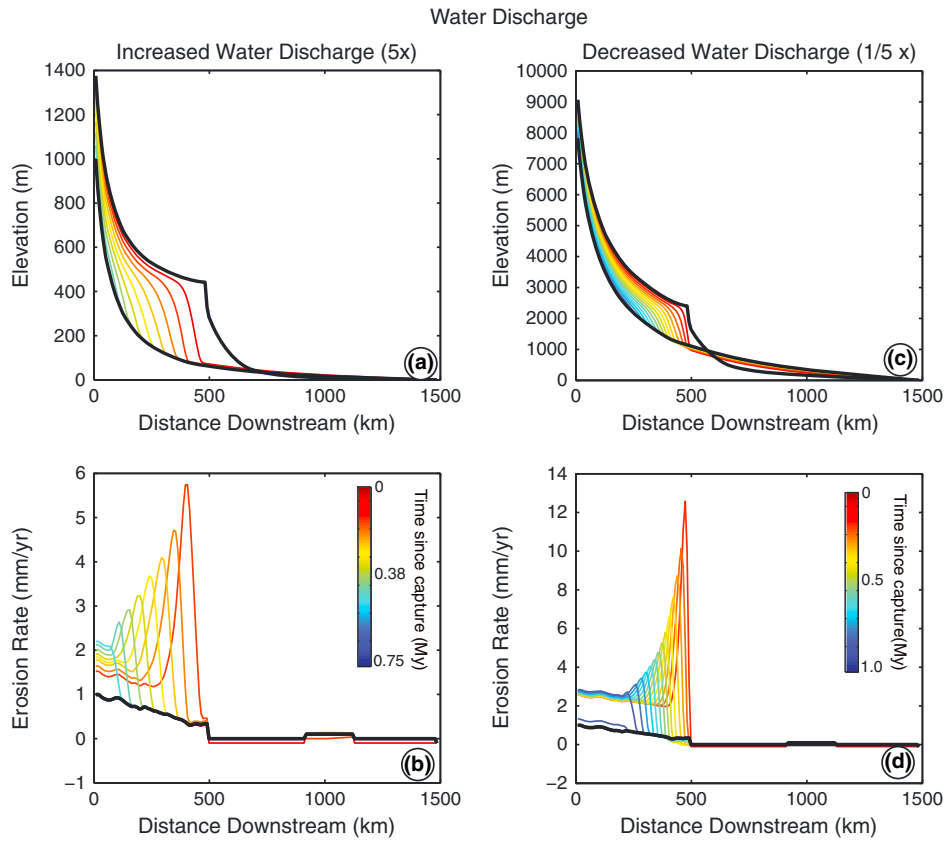

Figure 12. Model sensitivity to climate. The evolution of the river profile following capture for a fivefold (a) decrease and (c) increase in water discharge. Color of line denotes its age. Bold black lines are the pre-capture and post-capture steady state profiles. (b and d) The evolution of erosion rate. Note the similarities in both systems to Figure 7. Note the *y* axis scale varies in the subplots.

River (e.g., between glacial and interglacial cycles). Two end-member water discharge scenarios are simulated by varying the effective runoff parameter k_Q (Table 1) by factors of 5 and 0.2. Variations in water discharge exert a strong sensitivity on the magnitude of incision and moderate sensitivity on the maximum incision rate or timescale of adjustment. A fivefold increase in water discharge decreases the predicted magnitude of incision to ~375 m (Figure 12a), but the maximum erosion rate and the timescale of adjustment are lowered to only ~8.5 mm/yr (Figure 12b, note the differences in the scale of the *y* axes) and 500 kyr (Table 2), respectively. A fivefold decrease in discharge increases (relative to the baseline) the incision magnitude to ~1250 m (Figure 12c), the maximum erosion rate to 14.8 mm/yr (Figure 12d), and the timescale of adjustment to 800 kyr (Table 2). The difference in behavior is a result of the very different pre-capture steady state profiles (Figures 12a and 12c). The relief exhibited by the decreased water discharge experiment is unrealistically large suggesting that this value of water discharge is a lower end-member value. We note that

Table 2. Model Results

Run Name	Run Figure	Maximum Elevation Change (m)	Transience Timescale (Myr)	Maximum Erosion Rate (mm/yr)	% Difference Of Incision From Baseline
Baseline	Figures 7a–7c	726.4	0.7	11.4	0
Uniform uplift	Figures 8a and 8b	773.3	0.8	11.9	6.5
Lower subsidence	Figures 8c and 8d	730.8	0.75	11.4	0.6
$k_f = 10^{-3}$ m^{2}s/kg	Figures 9a and 9b	718.8	0.04	590.5	−1
$k_f = 10^{-4}$ m^{2}s/kg	Figures 9c and 9d	718.8	0.047	145.9	−1
$k_f = 10^{-6}$ m^{2}s/kg	Figures 9e and 9f	975	10.8	2.3	34.2
Variable lithology	Figures 9g and 9h	726.3	0.8	22.2	0
$D_{50} = 5$ cm	Figures 10a and 10b	214.8	0.45	5.1	−70.4
$D_{50} = 20$ cm	Figures 10c and 10d	2048.2	1.05	25.5	182
Uniform beta	Figures 10e and 10f	481.8	0.45	9.5	−33.7
Capture downstream	Figures 11a and 11b	1163.7	1	16.3	60.2
Capture upstream	Figures 11c and 11d	404.3	0.45	4.9	−44.3
Q_w increase	Figures 12a and 12b	377.5	0.5	8.5	−48
Q_w decrease	Figures 12c and 12d	1267.6	0.8	14.8	74.5

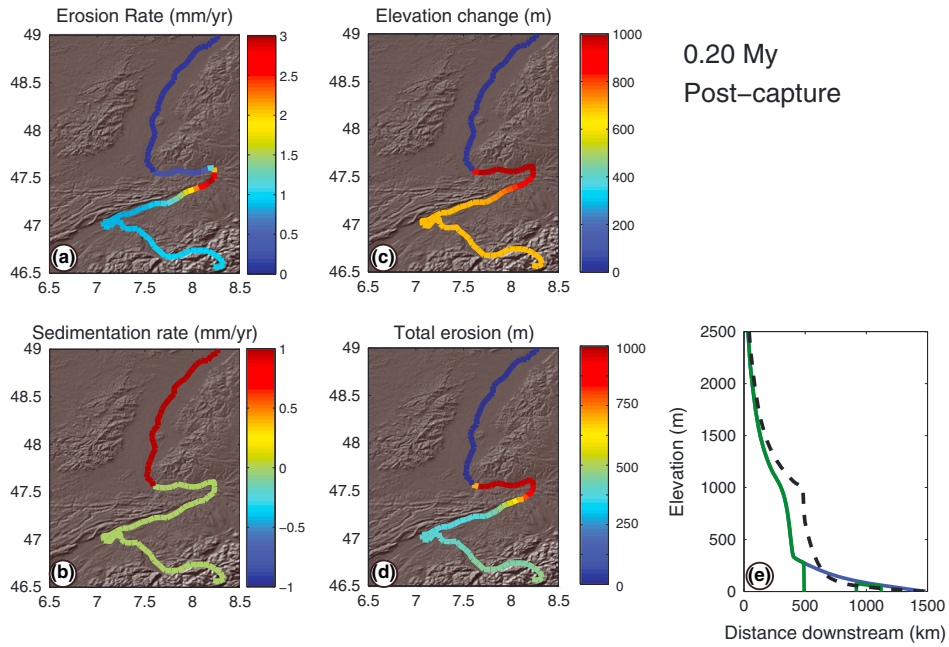

Figure 13. Image sequence showing the spatial distribution of river evolution due to drainage capture at 0.20 Myr following the capture event. See video in the auxiliary material for full illustration of the spatial evolution of the system. Model shown is the baseline model (Table 2 and Figure 7). (a) Snapshot of the instantaneous (one model time step) erosion rate; (b) snapshot of the instantaneous (one model time step) sedimentation rate; (c) elevation change since capture; (d) cumulative erosion since capture; and (e) snapshot of profile evolution. Dashed line is pre-capture steady state topography. Green line shows the bedrock surface, and blue line is where sediment is at the surface.

given the assumption of linear water discharge-precipitation scaling (see section 3.1) and a modern mean annual precipitation in the Rhine basin of ~630 mm, these values represent end-member climates with a mean annual precipitation of 130 mm and 3150 mm, well beyond a reasonable value for the Rhine Basin in the late Cenozoic.

5. Discussion: Application of Results to Northern Switzerland

[44] Drainage reorganization of the Rhine River has implications for landscape evolution of the Alpine Foreland in northern Switzerland and the central Alps as well as other regions where major drainage reorganization has occurred. The following discussion compares the model results with observations within the Rhine basin. This includes (1) the magnitude of Pliocene-modern erosion due to drainage capture, (2) the timing and magnitude of incision events along the Rhine River, and (3) the predicted model concavity and relief.

5.1. Implications for the Erosion of the Rhine River Basin

[45] This study provides a quantitative assessment of the impact of Rhine River reorganization on landscape evolution in Switzerland. The results suggest that drainage reorganization can account for a significant amount of Pliocene-modern incision within the Aare-Rhine River basin in the Alpine Foreland (Table 2) [*Mazurek et al.*, 2006; *Cederbom et al.*, 2011; *Schlunegger and Mosar*, 2011]. The model predictions are consistent with a number of observations in the region including (1) rapid pulses of incision and the abandonment of regional terrace levels [*Graf*, 1993; *Graf*, 2009; *Kock et al.*, 2009; *Preusser et al.*, 2011], (2) the magnitude of erosion through the Pliocene-Pleistocene in the Rhine and Danube basins [*Mazurek et al.*, 2006; *Willett and Schlunegger*, 2010], and (3) the pattern of erosion following terrace abandonment [*Preusser et al.*, 2011] (e.g., rather uniform upstream of the capture and decaying downstream of capture). We now discuss each of these predictions and the corresponding observations.

[46] In most model scenarios, the transient response to the drainage reorganization is considered to have occurred in less than 1 Myr of model time (Table 2 and Figures 7–12). The actual timescale of the entire incision event is likely longer since the reorganization occurred in a stepwise, time transgressive manner [*Ziegler and Fraefel*, 2009; *Villinger*, 1998, 2003]. Nonetheless, the rapidity of geomorphic response when drainage capture occurs is consistent with the regional abandonment of terrace levels in the Rhine basin. The preservation of spatially coherent relict deposits, such as the Deckenschotter (Figure 3) [*Frei*, 1912; *Graf*, 1993], is consistent with the pattern of erosion predicted by the model (Figure 13), though the magnitudes may vary (see section 5.2 below).

[47] The results demonstrate that a significant amount of Plio-Pleistocene erosion (a few hundreds of meters to 800 m) in the Rhine basin upstream of the capture location (Figure 1b) can be attributed to drainage reorganization. Spread over 4 Myr, this is equal to an average erosion rate 0.1–0.2 mm/yr. This magnitude of erosion accounts for a large part of the overall incision in the external Alpine Foreland (~1000 m according to *Cederbom et al.* [2011], *Müller et al.* [2002], and *Mazurek et al.* [2006]). It also accounts for an important fraction of erosion in the internal Alpine

Foreland and in the Alps over the last few million years [*Vernon et al*., 2008; *Glotzbach et al*., 2010, 2011a, 2011b; *Pignalosa et al*., 2011].

[48] As discussed in section 2, the elevation of the Blumberg gravels suggests that at least ~650 m of erosion has occurred since deposition (Figure 3). Moreover, Danube incision near the Blumberg gravels is only ~100 m (elevation between Blumberg gravels and modern Danube), which is much less than incision along the Rhine near Waldshut. This suggests that the erosional intensity in the Rhine basin has outpaced erosion rates in the Danube basin. Given the proximity (<50 km) of these locations, neither climate change nor broad-scale tectonics are likely to be the direct reason for such large differences in incision. The reorganization of drainages is most consistent with this difference in erosion. Essentially, the Rhine has an increased erosion capacity due to the increase in water discharge from capture, thereby causing the pirated Danube catchment to experience lower water discharge and a reduction in erosion. This is further evidenced by the migration of the drainage divide of the Danube, resulting in not only continued drainage area capture by the Rhine upstream of the Waldshut [e.g., *Morel et al*., 2003] but also drainage capture by the Neckar River along the northern drainage divide of the Danube [*Davis*, 1899; *Wagner*, 1929; *Hötzl*, 1996]. This effect will likely be a maximum at the upstream end, where the reduction in stream power along the Danube is greatest and wanes as the drainage area lost becomes insignificant downstream.

[49] The elevation of the Deckenschotter above modern river levels provides an estimate of incision since abandonment [*Müller et al*., 2002; *Preusser et al*., 2011]. The most recent major reorganization event is the redirection of the "Alpine Rhine" upstream of Lake Constance from the Danube to the Rhine system. The pattern of the Höhere Deckenschotter abandonment is consistent with this incision being driven by the reorganization. For example, minimum erosion occurs at the downstream end of the Deckenschotter (near Basel). Erosion then monotonically increases to about the recent outlet location of Lake Constance, where it levels off. Incision along the Aare system is also fairly uniform with values consistent with the erosion at the confluence near Waldshut. Exceptions to this pattern occur toward the internal Alpine Foreland (e.g., region of Lake Zurich), where incision magnitudes are greater. This pattern could result from either glacial overprinting from the Quaternary development of glacial overdeepenings or from increasing tectonic rock uplift toward the Alps. These observations are consistent with the pattern of river elevation change predicted by the modeling (Figures 7–13), where a maximum additional incision (beyond what is necessary to maintain steady state) occurs at the capture point and is propagated upstream. The magnitude of incision decays toward zero downstream of the capture location. Recall that total incision is the elevation change plus the incision needed to maintain topographic steady state. Therefore, where rock uplift is low (e.g., the northern part of the study area), the long-term incision pattern should mimic model predictions since the incision needed to maintain steady state is minimal; however, in areas of higher rock uplift (e.g., toward the Alps), the rate of rock uplift will accentuate the erosion magnitude recorded by the abandonment of the Deckenschotter in the foreland.

5.2. Implications of Multiple Capture Events for Landscape Evolution in the Rhine River Basin

[50] The single river capture event simulations presented so far are useful for understanding the effects of capture on river incision and analyzing the sensitivity to model parameters; however, the history of the reorganization is decidedly more complicated than the models described above. Three major events are generally accepted concerning capture around the Rhine River (in order of occurrence):

[51] 1. An Aare-Danube system was captured near the modern confluence of the Aare-Rhine (specifically the Hochrhine near Waldshut) creating an Aare-Doubs River system draining to the Mediterranean. This occurred sometime around/before 4.2 Ma based on fossils in the Sundgau gravels dated to 4.2–2.9 Ma [*Petit et al*., 1996].

[52] 2. The Aare-Doubs system was captured in the area north of the city of Basel, Switzerland (Figure 1) and formed the first connections between the Swiss Alps, the Central and Northern Upper Rhine Graben, and the North Sea (2.9–1.7 Ma based on the arrival of central Alpine mineral assemblages dated to 2.6 Ma [*Weidenfeller and Knipping*, 2008; *Hoselmann*, 2008] and the Sundgau gravels being not older than 2.9 Ma [*Petit et al*., 1996].

[53] 3. The Alpine Rhine upstream of Lake Constance was integrated into the Hochrhine and Aare-Rhine and thus into the the North Sea flowing Rhine sometime between 1.7 and 0.8 Ma [*Ziegler and Fraefel*, 2009; *Preusser et al*., 2011]. Note that the Alpine Rhine integration may have occurred in a two-stage process where at least half of the system was integrated through the Walensee channel (through the region of Zürich to Waldshut). This was then followed by the integration of the region around Lake Constance (Figure 1). Without direct evidence that dates the integration of these sub-basins, we will assume the entire Alpine Rhine is captured in only one stage.

[54] To illustrate the potential impact of this more complicated drainage history, we simulate these three events successively using our drainage capture model. The methods for modeling the multiple capture events can be found in section B.

[55] The results presented in Figure 14 highlight the complexity of these multiple capture events on landscape evolution in northern Switzerland and the Alps. Each event generates landscape transience, but the size of the erosion signal varies. For example, the reorganization of the Aare-Danube to the Aare-Doubs (event 1) generates in the model an ~500 m wave of incision up the Aare (Figure 14a). The subsequent rearrangement through the Upper Rhine Graben 1.3 My later sends another pulse of incision of ~ 220 m upstream through the Rhine-Aare system (Figure 14b). Finally, the integration of the Alpine Rhine 1.9 My later generates another ~40 m of incision along the Aare-Rhine river system. The 40 m incision magnitude decays from the location of Waldshut to ~0 m at Basel (note this is not plotted due to the small magnitude of elevation change relative to line thickness in Figure 14). Although not investigated here, all of these events would have interesting implications for temporarily increasing incision rates of tributary rivers and enhanced hillslope erosion rates near the capture location (Figures 1 and 13).

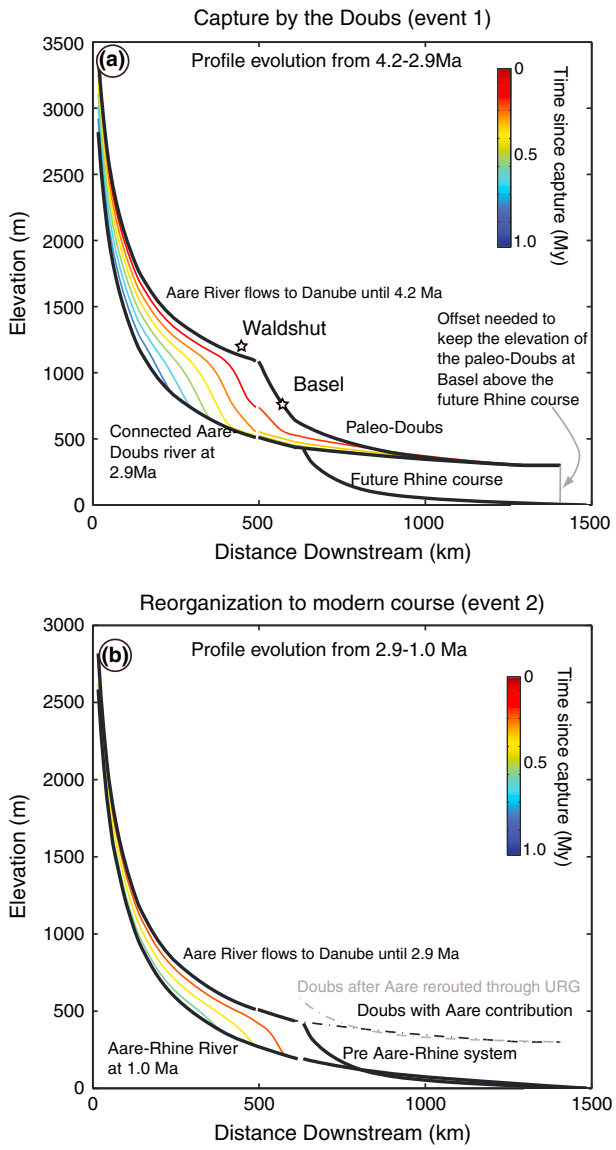

Figure 14. The impacts of multiple drainage reorganization events on river profile evolution. See Figure 1 for capture locations. (a) Capture of the paleo-Aare-Danube by the Doubs at ~4.2 Ma. (b) Capture of the paleo-Aare-Doubs by the modern course of the Rhine River at ~2.9 Ma.

[56] The modeled results are consistent with the abandonment of at least three terrace levels or gravel deposits. Although the ages of terrace and gravel deposits are poorly constrained, we can make some inferences based upon what is known. The abandonment of the Blumberg gravels (~600 m above modern Rhine River and ~300 m above the next terrace level; Figure 3) is most consistent with the capture of the Aare-Danube by the paleo-Doubs. The step between the Höhere (higher) and Tiefere (lower) Deckenschotter (~50–100 m elevation difference; Figure 3), or possibly the abandonment of the Tiefere Deckenschotter (~50–200 m above modern river; Figure 3), may be associated with the capture of the Alpine Rhine [*Preusser et al.*, 2011], which is likely to have happened somewhere between Waldshut and Lake Constance. Consequently, erosion would be a maximum in this region (capture location) and decay downstream. However, the lack of precise dating of these deposits limits our ability to definitively tie them to distinct drainage reorganization events. The timing, place, and course of action of the capture of the Alpine Rhine are debated [cf. *Villinger*, 2003; *Preusser*, 2008; *Keller*, 2009; *Ziegler and Fraefel*, 2009]. The elevation differences between the terrace levels show a similar pattern to the model results which predicts incision of ~500, 220, and 40 m for the three modeled events. We note that the mismatch between the modeled and observed incision is well within uncertainty in estimates of model parameters. Despite the simplified modeling approach with three main capture events, our results show that some of the major steps between terrace levels in northern Switzerland may be related to major drainage reorganizations.

5.3. Additional Considerations

5.3.1. Potential Influence of Glacial-Interglacial Cycles on Results

[57] It is clear that glacial processes have overprinted fluvial morphology in the upper reaches of the Rhine [e.g., *Norton et al.*, 2008]. Whether or not the incision wave due to any of the capture events influenced the erosional budget of the high Alps depends on the timing of the reorganization events relative to the onset of glaciation and the magnitude of glacial erosion. For example, if glaciers formed and were erosive enough to lower valley elevations prior to the arrival of the capture signal, then glacial overprinting could reduce the magnitude of the incisional wave when it arrives in the core of the Alps. Given that the timing of the first capture event is ~4.2 Ma, well before extensive Alpine glaciations [*Muttoni et al.*, 2003], and that the incision likely worked its way through the landscape in 1 Myr (so by 3.2 Ma), at least some of the Pliocene-modern exhumation of the central Alps is due to this capture event [*Schlunegger and Mosar*, 2011]. As the first known major glacial advance in the Swiss Alps occurred during the mid-Pleistocene revolution at around 0.87 Ma [*Muttoni et al.*, 2003], we expect that most of the incision propagated through much of the Alps before being strongly influenced by glacial processes. Furthermore, even with glaciers in the Alps, the base level lowering that is generated by this incision event will propagate to the glaciated part of the landscape, potentially influencing the type and rate of glacial erosion [e.g., *Shuster et al.*, 2011].

[58] Glacial-interglacial cycles have undoubtedly influenced sediment and water discharge over timescales of tens to hundreds kiloyears. Climate was generally drier during glacial periods, potentially with up to 60% less precipitation [*Peyron et al.*, 1998], thus our calculated response times based on modern climate are likely minima. Changes in grain size during glacial times are not constrained along the Rhine River. If glacial periods produce coarser sediment, this would slow the transient response timescale (Table 2); however, the initial profiles and initial transient waves developed prior to Alpine glaciation and therefore not influenced by glacially driven fluctuations in grain size. Further constraints on the evolution of Aare-Rhine grain size over the last 4 Myr will improve the ability to model fluvial response to drainage organization. Without this information, we kept water discharge and sediment characteristics steady through the simulation. This implicitly assumes that the effects of this

variability average out over multiple glacial-interglacial timescales.

[59] Sea level variation is another potential control on fluvial erosion in the Rhine basin, though we note that the base level effects of sea level depend on the slope of the continental shelf. Given that the slope of the Rhine Delta is similar to the slope of the lower Rhine [*Törnqvist et al.*, 2000], we do not expect variations in base level from sea level change to be significant. We also note the rock uplift history and pattern are not well known in central Europe. Our model, however, shows limited sensitivity for the evolution of the river profile, the maximum erosion rate, and profile adjustment time to rock uplift patterns (Figure 8), suggesting that our results remain robust.

5.3.2. Flexure and Tectonics

[60] Our modeling does not include the flexural isostatic response of the crust to the migrating wave of incision. As the flexural response is a function of the total mass removed, this calculation would require modeling the transience into the tributaries and hillslopes of the Rhine, which is beyond the scope of this study. As an end-member, we can assume full isostatic compensation and calculate additional rock uplift due to the incision. Removing 700 m of mass from the surface will cause a rebound of about 570 m (for a lithosphere-asthenosphere density ratio of 2700/3300 kg/m^3). This additional rock uplift would drive more erosion providing a feedback; however, >1.5 km of incision in the external foreland is beyond any reasonable estimate based on geologic observations [*Cederbom et al.*, 2011; *Müller et al.*, 2002; *Mazurek et al.*, 2006]. There are a number of reasons that this can be considered an overestimate to the contribution of capture to the rock uplift of the Alps and foreland. For example, it ignores any flexural support which lowers the magnitude of rock uplift in response to unloading. Also, transient waves tend to slow down as drainage area decreases (*Rosenbloom and Anderson* [1994] and the sensitivity test of lower water discharge). Therefore, the transience may still be actively occurring in the tributaries and on the hillslopes, and therefore, the average amount of unloading across the whole landscape is clearly <700 m. And finally, glacial processes may have overprinted the river capture contribution. This simple calculation of isostatic rebound does, however, reveal the importance of how the evolution of base level in the foreland can have profound impacts on the exhumation of the adjoining orogen, especially if the orogen is in a state of decay. Not only is this important for understanding the drivers of Alpine exhumation, but it is also important for other orogens where drainage reorganization events have occurred.

[61] The Jura was tectonically active between 10 and 4 Ma [*Ziegler and Fraefel*, 2009], with some evidence suggesting continued deformation today [*Madritsch et al.*, 2009]. By assuming a steady rate of rock uplift, we have likely oversimplified the tectonic history of the region, both spatially and temporally. However, given our inability to constrain past rock uplift rates, we use the modern data to constrain the general trend of rock uplift [*Gubler et al.*, 1981; *Schlatter et al.*, 2004] along the river profile. Moreover, the limited sensitivity of our modeling to large-scale rock uplift variations (Figure 8) suggest that non-steady tectonic processes would have minimal impact on incision driven by drainage reorganization. Spatially, local tectonic processes (e.g., thrusting and folding in the Jura Mountains) will certainly have an impact on total incision on a local scale. However, the impact on the shape of the large-scale river profile will be small.

5.3.3. Driving Mechanisms

[62] The modeling approach presented here forces the capture to occur at a specified time without a driving mechanism initiating the capture. Various mechanisms have been proposed to drive drainage reorganization in the Alps [*Ziegler and Fraefel*, 2009; *Schlunegger and Mosar*, 2011] and elsewhere [*Bishop*, 1995; *Brocard et al.*, 2012]. Such physical mechanisms include tectonic activity, ice sheets, landslides, and groundwater processes.

[63] Although many of these processes are plausible causes of drainage reorganization in the Alpine Foreland, our preferred mechanism for the capture of the Aare-Danube to the paleo-Doubs is groundwater sapping. The evidence in support of this mechanism include (1) the point of capture occurred in an area where limestone bedrock is common; (2) the capture of the Aare-Danube occurred before the development of large ice sheets; (3) there is evidence of ongoing capture occurring at many locations along the Danube divide including Danube capture by the Neckar basin [*Davis*, 1899] where tectonics, ice sheet, and landslide mechanisms are unlikely; and (4) the Blumberg gravels are deposited on the Malm limestone, which strikes NE-SW from Blumberg to Waldshut. This is the same unit in which considerable flow along the modern Danube River is lost through karst systems to the Rhine in the region north of Lake Constance [*Hötzl*, 1996]. If this hypothesis is correct, it has important implications for the controls on exhumation in orogens such as the Alps. Essentially, the drainage reorganization is a result of the natural progression of internal dynamics between the hydrologic and geomorphic systems, and therefore, the incision wave cannot be tied to any one specific tectonic or climatic cause. Future work is clearly needed to address how these drainage organization events occur.

[64] Of course a prerequisite for groundwater sapping is the existence of a catchment with a lower base level close to the Aare-Danube course. It is possible that a lowering of river elevations in the neighboring basins helped facilitate the groundwater-sapping processes. A low base level and a growing drainage area of the paleo-Doubs catchment could have resulted from the Messinian salinity crisis, a period of low sea level in the Mediterranean from ~6.0 to 5.3 Ma. This event caused the incision of deep gorges in the Rhone valley [*Gargani*, 2004]. Taking into account the large uncertainty of the age of the Aare-Danube capture event (~4.2 Ma), and the relatively long distance between the Mediterranean and paleo-Doubs capture location, this scenario is quite possible.

[65] Even though all capture locations are located near limestone bedrock, influences from other mechanisms for capture are possible. For example, the second capture (Aare-Doubs capture by the paleo-Rhine) is located within the Upper Rhine Graben, and therefore a tectonic cause for the capture is plausible [*Hötzl*, 1996; *Ziegler and Fraefel*, 2009; *Schlunegger and Mosar*, 2011]. Finally, given the mid-Pleistocene timing of the reorganization of the Alpine Rhine, we suspect glacial landscape processes played a role in the integration of the Alpine Rhine into the Aare-Rhine system [e.g., *Keller*, 2009].

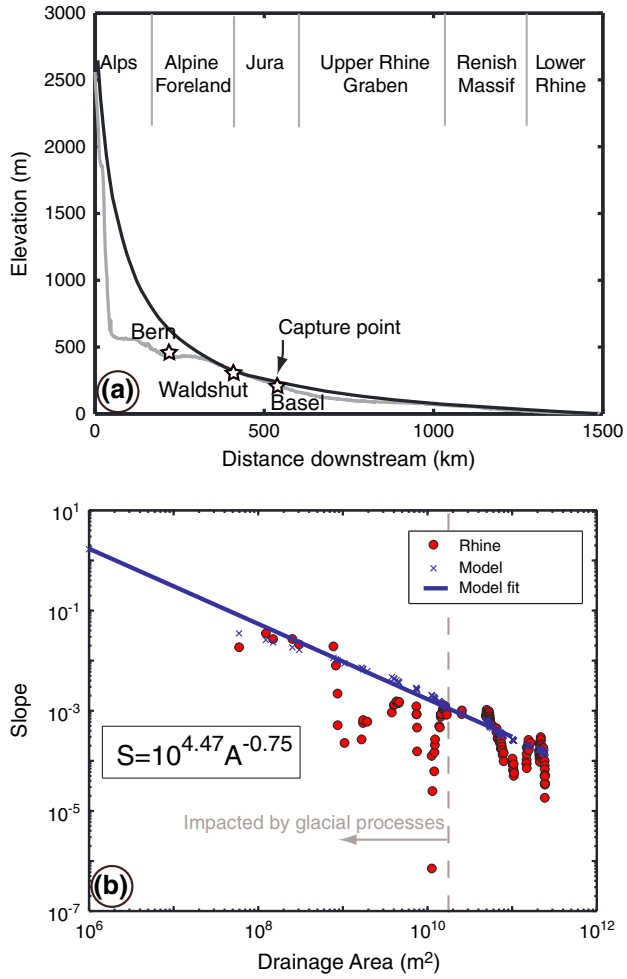

Figure 15. Morphological comparison between modern and modeled Rhine River. (a) Comparison between the baseline model (black) profile and the modern Rhine River (grey). The modern Rhine above ~500 m has been heavily influenced by late Quaternary glaciations. (b) Comparison of Rhine River slope area data (red circles) to simulated slope area (blue crosses). Simulated profile matches the Rhine reasonably well. Note that many of the deviations upstream of 10^{10} m^2 result from glacial overprinting.

5.4. Model Validation

[66] The analysis presented here reproduces many geomorphic characteristics of the river systems including the rate of incision following a capture event, fluvial relief, and river concavity. For example, estimates of the transient response of the Wutach River capture suggest a short-lived erosion pulse of 25 mm/a following the capture [*Einsele and Ricken*, 1995]. This is consistent with our estimated values of maximum incision (Figure 7 and Table 2) for the time intervals analyzed. The morphologies of the modeled and modern river profile are also consistent (Figure 15). In Figure 15, we plot the slope and area of the modern Rhine River as well as the slope-area relationship for the final steady state river profile shown in Figure 7. The slope of the regression line is the river concavity, which is consistent between the modeled (0.75) and modern Rhine River (0.69). This scaling persists even when ignoring the glacially modified portion of the landscape along the Aare-Rhine (Figure 1) corresponding to a drainage area of less than ~10^{10} m^2 (Figure 15). River concavity is sensitive to patterns in rock uplift/subsidence, sediment supply, and downstream changes in grain size [*Sinha and Parker*, 1996; *Gasparini et al.*, 2004]. Because multiple parameters control concavity, its value is not unique with regard to any one factor; however, combined with the reproduction of fluvial relief and predictions of incision magnitude consistent with observed incision since the drainage reorganization, we are confident that the model captures, at least to the first order, the impacts of drainage reorganization on the evolution of the Rhine River in Switzerland over the last few million years. This suggests that a simple shear stress river erosion model, when accounting for sediment transport, can roughly capture river morphodynamics and the impacts of drainage capture along the Rhine River.

[67] Estimates of a lower magnitude of erosion (e.g., from small grain size) occur when the initial and final profiles have reliefs that are quite low compared to the modern Rhine. Such profiles are not consistent with the modern relief along the Rhine. Simulations that reproduce the modern Rhine profile relatively well require at least 400 m of erosion following drainage reorganization. It therefore seems plausible that in order to develop the modern Rhine profile, incision due to drainage capture must have occurred. This is consistent with the elevation of multiple terrace levels in the Rhine Basins, both upstream and downstream of the capture location.

6. Conclusions

[68] The history of drainage basin evolution in central Europe since the early Pliocene has important implications for the evolution of the Alps and Alpine Foreland. To explore the effects of drainage reorganization on landscape evolution, we modeled the fluvial response to the rerouting of the paleo-Aare-Danube River system to its modern course. We used a simple 1-D model of sediment transport and river erosion with the assumption that the elevation of the upstream river (Aare-Danube) at the capture location must have been higher than the point of capture on the downstream river profile. We found that drainage reorganization along the Rhine River in central Europe could have generated more than 400 m of incision upstream of Basel (Waldshut area, Switzerland; Figure 1). The sensitivity of results to model parameters was tested and showed that sediment characteristics (e.g., grain size, bed load proportion) strongly influenced the river dynamics, though all of these scenarios still predict at least several hundred meters to a kilometer of incision. Regional variations in tectonically driven rock uplift are found to have minimum effects on modeled river profile evolution. In any case, drainage reorganization can account for a considerable part of the incision measured in the external Alpine Foreland over the last few million years. The transience from these events rapidly swept through the fluvial reaches upstream of the capture location, most likely in less than one million years. This incisional wave also reached the Alps and influenced exhumation, but the magnitude of the drainage reorganization incision in the Alps is likely less than uplift-induced erosion and glacial processes in the late Pleistocene. It is clear that

the incisional response of the Rhine River to drainage reorganization must be considered in accounting for controls on Quaternary landscape evolution in this region.

Appendix A

A.1. Baseline Model Parameters

[69] An initial set of parameters for the previous equations were chosen as representative values for the modern Rhine River (Table 1). The simulation conducted with these parameters is hereafter referred to as the baseline model and the reference point for comparison with our other simulations. Most of these values were selected from previously published studies (Table 1). Some values were calculated here, such as bedrock erodibility, such that river profiles similar to the modern shape and relief of the Rhine River evolved from the numerical model. A summary of the model parameters and the rational for using them are found below and in Table 1.

A.1.1. Uplift and Subsidence Histories

[70] River erosion is sensitive to the rate of base level fall (the relative vertical movement of the downstream end of a given river reach), which is largely controlled by rock uplift patterns [*Whipple and Tucker*, 1999]. Rock uplift patterns in the Alps, Upper Rhine Graben, Rhenish Massif, and Lower Rhine Graben are estimated from a number of observations (Figure 5). For example, leveling lines constrain the rate of rock uplift relative to Basel for much of Switzerland [*Schlatter et al*., 2005; *Gubler et al*., 1981]. The measurements suggest a maximum of ~1 mm/yr in the core of the Alps and a decline to a reference point located about 40 km east of Basel, where the Rhine flows on crystalline basement of the Black Forest Massif [*Schlatter et al*., 2005]. Rates of sediment accumulation in the Upper Rhine Graben and Lower Rhine Graben provide long-term estimates of subsidence rates. The maximum thickness of Quaternary sediments in the Upper Rhine Graben was reported to be around 380 m [*Bartz*, 1953] and can be as low at 50 m [*Hagedorn and Boenigk*, 2008]. We choose a uniform value of ~0.1 mm/yr subsidence as it represents an average value. We also choose 0.1 mm/yr subsidence in the Lower Rhine Graben based on average Quaternary sediment thickness [*Zagwijn*, 1989]. Little information exists on rock uplift in the Rhenish Massif, but ~80 m of incision has taken place since the mid-Pleistocene, which is consistent with a rock uplift rate of 0.1 mm/yr [*Boenigk and Frechen*, 2006].

A.1.2. Geomorphic Variables

[71] Consistent gauging records along the Rhine exist since the early twentieth century. *Pinter et al*., [2006] compiled average annual maximum discharge for 10 gauging stations between Rheinfelden, Switzerland, and Rees, Germany. Regressing the average maximum discharge with drainage area results in a scaling, k_Q (see Table 1, discharge scaling), of $\sim 10^{-8}$ ($r^2 = 0.97$) for a linear relationship. A nonlinear relationship also fits the data (power of 0.7) but it is difficult to know how much of this relationship has been affected by anthropogenic modification. Given the high r^2 value on the linear regression, we chose this simpler model for the relationship between drainage area and water discharge. We chose a coefficient of 2×10^{-8}. Over an entire year, this value is volumetrically equivalent to a mean annual precipitation of 628 mm, which is consistent with observations in the Rhine River basin [*Frei and Schär*, 1998] although this value has likely varied over glacial-interglacial periods (see discussion in section 5.3).

[72] We assume a channel width to discharge exponent of 0.5, a value common to many empirical and theoretical studies [*Wohl and David*, 2008; *Finnegan et al*., 2005, *Montgomery and Gran*, 2001; *Yanites and Tucker*, 2010]. The channel width coefficient was selected to provide reasonable width values along the entire flow length of the Rhine (Figure 5). For example, channel widths measured from Google Earth measure 70 m at Bern and 250 m at Basel. We note however that these values are likely less than bankfull flood stage. Therefore, we choose values to produce a width of ~100 m at Bern and ~400 m at Basel. A more detailed analysis is not possible due to anthropogenic modification of the river.

[73] Quantifying the resistance of bedrock to erosion processes along the Rhine is a challenging problem. In other river basins, researchers calibrating river erosion models have shown that erodibility values can vary over many orders of magnitude [e.g., *Stock and Montgomery*, 1999; *Yanites et al*., 2010]; however, no river erosion calibration study has been performed for Alpine and foreland rivers. Therefore, we rely on the geomorphic constraint of fluvial relief to choose a baseline erodibility as fluvial relief is sensitive to the erodibility [*Whipple and Tucker*, 1999].

A.1.3. Grain Size

[74] Previous work has constrained sediment characteristics as a function of distance downstream. For example, *Mikos* [1994] estimated abrasion coefficients for Sternberg's law that describes the evolution of grain size as a function of distance downstream (Figure 5 and Table 1) along the Alpine Rhine. We found that assuming an initial (0 km) grain size of 10 cm and a grain size reduction factor of 0.005 best reproduced the available data. This predicts, for example, the observed mean grain size of 6 cm at 20 km from the headwaters [*Mikos*, 1994]. Note that we are assuming an equivalency between mean and median grain size; however, the differences between them are likely much smaller than the methodological uncertainty.

B. Multiple Capture Methods

[75] To accomplish this, we extract the river profile of the Doubs River from a location near the modern divide with the Rhine (Figure 1b) to the city of Lyon, France, where Pliocene marine sediments are found. The section of the modern Aare-Rhine river between the capture by the paleo-Doubs and the Upper Rhine Graben (i.e., the reach between Waldshut and Basel; Figure 1) was initially added to the paleo-Doubs River to simulate the geography at this time [*Ziegler and Fraefel*, 2009]. Therefore, three initial river profiles are simulated: (1) the Aare River from its headwaters to the town of Waldshut; (2) the Doubs, which comprises the Rhine from approximately Waldshut to Basel and extrapolated to the modern location of the Doubs near the divide; and (3) the Rhine River from the Upper Rhine Graben (starting downstream of Basel) to the North Sea. We exclude the drainage area represented by the Alpine Rhine upstream of Lake Constance since this was not integrated until the middle Quaternary (event 3 from above). Therefore, the first two events are simulated with the drainage area of the Alpine Rhine subtracted from all river locations downstream of the modern confluence of the

Aare-Rhine (specifically the Hochrhine) near Waldshut. The first event is the connection of the Aare River with the paleo-Doubs at ~4.2 Ma (Figure 14). This system (i.e., the Aare-Doubs River) evolves for 1.3 Myr until the paleo-Rhine captures the Aare River near Basel (Figure 14) at ~2.9 Ma, forming the Aare-Rhine. This profile evolves for ~1.9 Myr. The final event represents the Alpine Rhine (upstream of Lake Constance) integration by adding the drainage area upstream of Lake Constance at 1 Ma.

[76] The capture of the Aare-Doubs system by the paleo-Rhine at 2.9 Ma (event 2) requires that the Aare-Doubs river at the point of capture is at a higher elevation than the capture point along the paleo-Rhine located downstream of Basel. To ensure this happens, we offset the base level for the Doubs River until this condition is satisfied (Figure 14a). It is possible that this condition could be met by tuning another model parameter such as grain size or water discharge along the paleo-Doubs; however, for simplicity and model comparison purposes, we chose to keep parameters consistent between modeled profiles. Because of this constraint, our model results should be considered maximum estimates. The Doubs profile is given a rock uplift rate of 0.05 mm/yr [*Madritsch et al.*, 2009], except for the Bresse Graben where we assume a subsidence of 0.1 mm/yr. All other parameters are the same as Table 1.

[77] **Acknowledgments.** We are grateful to H. Madritsch, for stimulating discussions concerning the geologic and geomorphic evolution of the Rhine Catchment. Thoughtful reviews by P. Prince, M. Hinderer, F. Schlunegger, Associate Editor Brocklehurst, and Editor Densmore greatly improved this manuscript.

References

Andrews, G. D. M., J. K. Russell, S. R. Brown, and R. J. Enkin (2012), Pleistocene reversal of the Fraser River, British Columbia, *Geology*, doi:10.1130/G32488.1.

Barnes, H. H. (1967), Roughness characteristics of natural channels, *U.S. Geol. Sur. Water-Supply Pap.*, *1849*, 213.

Bartz, J. (1953), Revision des Bohrprofils der Heidelberger Radium-Sol-Therme. Jahresberichte und Mitteilungen des Oberrheinischen Geologischen Vereines N.F. 33: 101–125.

Beranek, L. P., P. K. Link, and C. M. Fanning (2006), Miocene to Holocene landscape evolution of the western Snake River Plain region, Idaho: Using the SHRIMP detrital zircon provenance record to track eastward migration of the Yellowstone hotspot, *Geol. Soc. Am. Bull.*, *118*, doi:10.1130/B25896.1.

Berger, J.-P., B. Reichenbacher, D. Becker, M. Grimm, K. Grimm, L. Picot, A. Storni, C. Pirkenseer, C. Derer, and A. Schaefer (2005), Paleogeography of the Upper Rhine Graben (URG) and the Swiss Molasse Basin (SMB) from Eocene to Pliocene, *Int. J. Earth Sci. (Geol. Rundsch)*, *94*, doi:10.1007/s00531-005-0475-2.

Bishop, P. (1995), Drainage rearrangement by river capture, beheading and diversion, *Progr. Phys. Geogr.*, *19*(4), 449–473, doi:10.1177/030913339501900402.

Bitterli-Dreher, P., H. R. Graf, H. Naef, P. Diebold, F. Matousek, and H. Burger (2007), Blatt Baden (1070/120)—Erläuterungen, Geologischer Atlas der Schweiz 1:25,000, *Bundesamt für Landestopografie swisstopo*.

Boenigk, W., and M. Frechen (2006), The Pliocene and Quaternary fluvial archives of the Rhine system, *Quat. Sci. Rev.*, *25*, doi:10.1016/j.quascirev.2005.01.018.

Boenigk, W. (1987), Petrographische Untersuchungen jungtertiärer und quartärer Sedimente am linken Oberrhein, Jahresberichte und Mitteilungen des oberrheinischen geologischen, *Vereins*, *69*, 357–394.

Bolliger, T., O. Fejfar, H. Graf, and D. Kaelin (1996), Vorläufige Mitteilung über Funde von pliozänen Kleinsäugern aus den höheren Deckenschottern des Irchels (Kt. Zürich), *Eclogae Geol. Helv.*, *89*, 1043–1048.

Brocard, G., et al. (2012), Rate and processes of river network rearrangement during incipient faulting: The case of the Cahabón River, Guatemala, *Am. J. Sci.*, *312*, doi:10.2475/05.2012.01.

Carling, P. A. (1989), Bedload transport in two gravel-bedded streams, *Earth Surf. Process. Landforms*, *14*, 27–39, doi:10.1002/esp.3290140104.

Cederbom, C. E., P. van der Beek, F. Schlunegger, H. D. Sinclair, and O. Oncken (2011), Rapid extensive erosion of the North Alpine foreland basin at 5–4 Ma, *Basin Res.*, *23*, doi:10.1111/j.1365-2117.2011.00501.x.

Champagnac, J. D., P. Molnar, R. S. Anderson, C. Sue, and B. Delacou (2007), Quaternary erosion-induced isostatic rebound in the western Alps, *Geology*, *35*, doi:10.1130/G23053A.1.

Chow, V. T. (1959), *Open-Channel Hydraulics*, McGraw-Hill, New York, NY.

Clark, M. K., L. M. Schoenbohm, L. H. Royden, K. X. Whipple, B. C. Burchfiel, X. Zhang, W. Tang, E. Wang, and L. Chen (2004), Surface uplift, tectonics, and erosion of eastern Tibet from large-scale drainage patterns, *Tectonics*, *23*, TC1006, doi:10.1029/2002TC001402.

Clift, P. D., and J. Blusztajn (2005), Reorganization of the western Himalayan river system after five million years ago, *Nature*, *438*, doi:10.1038/nature04379.

Craddock, W. H., E. Kirby, N. W. Harkins, H. Zhang, X. Shi, and J. Liu (2010), Rapid fluvial incision along the Yellow River during headward basin integration, *Nat. Geosci.*, *3*, doi:10.1038/ngeo777.

Davis, W. M. (1899), The drainage of cuestas, *Proc. Geol. Assoc.*, *16*, 75–93.

Einsele, G., and W. Ricken (1995), The Wutach gorge in SW Germany: Late Würmian (periglacial) downcutting versus Holocene processes, *Z. Geomorphol. (Suppl.)Band*, *100*, 65–87.

Ellwanger, D., J. Lämmermann-Bartherl, and I. Neeb (2003), Eine landsschaftsübergreifende Lockergesteinsgliederung vom Alpenrand zum Oberrhein, *Landschaftsgeschichte im europäischen Rheinland, GeoArcheoRhein*, *4*, 81–124.

Farr, T. G., et al. (2007), The Shuttle Radar Topography Mission, *Rev. Geophys.*, *45*, RG2004, doi:10.1029/2005RG000183.

Finnegan, N. J., G. Roe, D. R. Montgomery, and B. Hallet (2005), Controls on the channel width of rivers: Implications for modeling fluvial incision of bedrock, *Geology*, *33*, doi:10.1130/G21171.1.

Frei, R. (1912), Monographie des Schweizerischen Deckenschotters. Beiträge zur Geologischen Karte der Schweiz, *Geologische Kommission der Schweizerischen Naturforschenden Gesellschaft*.

Frei, C., and Schär, C. (1998), A precipitation climatology of the Alps from high-resolution rain-gauge observations, *Int. J. Climatol.*, *18*, 873–900.

Gargani, J. (2004), Modelling of the erosion in the Rhone valley during the Messinian crisis (France), *Quat. Int.*, *121*, doi:10.1016/j.quaint.2004.01.020.

Gasparini, N. M., G. E. Tucker, and R. L. Bras (2004), Network-scale dynamics of grain-size sorting: Implications for downstream fining, stream-profile concavity, and drainage basin morphology, *Earth Surf. Processes Landforms*, *29*, doi:10.1002/esp.1031.

Giamboni, M., A. Wetzel, B. Nivière, and M. Schumacher (2004), Plio-Pleistocene folding in the southern Rhinegraben recorded by the evolution of the drainage network (Sundgau area; northwestern Switzerland and France), *Eclogae Geol. Helv.*, *97*.

Glotzbach, C., P. A. van der Beek, and C. Spiegel (2011a), Episodic exhumation and relief growth in the Mont Blanc massif, Western Alps from numerical modelling of thermochronology data, *Earth Planet. Sci. Lett.*, *304*, doi:10.1016/j.epsl.2011.02.020.

Glotzbach, C., M. Bernet, and P. van der Beek (2011b), Detrital thermochronology records changing source areas and steady exhumation in the Western European Alps, *Geology*, *39*, doi:10.1130/G31757.1.

Glotzbach, C., J. Reinecker, M. Danišík, M. Rahn, W. Frisch, and C. Spiegel (2010), Thermal history of the central Gotthard and Aar massifs, European Alps: Evidence for steady state, long-term exhumation, *J. Geophys. Res.*, *115*, F03017, doi:10.1029/2009JF001304.

Graf, H. R. (1993), Die Deckenschotter der Zentralen Nordschweiz, ETH Zürich.

Graf, H. R. (2009), Stratigraphie von Mittel- und Spätpleistozän in der Nordschweiz - Beiträge zur Geologischen Karte der Schweiz (N. F. 168), *Swiss Geological Survey*, Federal Office of Topography swisstopo.

Gray, H. H. (1991), Origin and history of the Teays drainage system: The view from midstream, in *Geology and Hydrogeology of the Teays-Mahoment Bedrock Valley System*, edited by W. N. Melhorn, and K. P. Kempton, Colorado, Geological Society of America Special Paper 258, Boulder, Geological Society of America, 43–50, doi:10.1130/SPE258-p43.

Gubler, E., H.-G. Kahle, E. Klingelé, S. Mueller, and R. Olivier (1981), Recent crustal movements in Switzerland and their geophysical interpretation, *Tectonophysics*, *71*, 125–152, doi:10.1016/0040-1951(81)90054-8.

Gunnell, Y., and D. J. Harbor (2010), Butte detachment: How pre-rift geological structure and drainage integration drive escarpment evolution at rifted continental margins, *Earth Surf. Processes Landforms*, *35*, doi:10.1002/esp.1973.

Hagedorn, E.-M. (2004), Sedimentpetrographie und Lithofazies der Jungtertiären und Quartären Sedimente im Oberrheingebiet, P*hD thesis, Universität zu Köln*.

Hagedorn, E. M., and W. Boenigk (2008), The Pliocene and Quaternary sedimentary and fluvial history in the Upper Rhine Graben based on heavy mineral analyses, *Neth. J. Geosci.*, *87*.

Hebestreit, C. (1995), Zur jungpleistozänen und holozänen Entwicklung der Wutach (SW-Deutschland), *Tübinger Geowissenschaftliche Arbeiten*, *C25*, 88.

Hofmann, F. (1996), Zur plio-pleistozänen Landschaftsgeschichte im Gebiet Hochrhein-Wutach-Randen-Donau: Geomorphologische Überlegungen und sedimentpetrographische Befunde, *Eclogae Geol. Helv.*, *89*, 1023–1041.

Hoselmann, C. (2008), The Pliocene and Pleistocene fluvial evolution in the northern Upper Rhine Graben based on results of the research borehole at Viernheim (Hessen, Germany), *Quat. Sci. J.*, *57*.

Hötzl, H. (1996), Origin of the Danube-Aach system, *Environ. Geol.*, *27*, 87–96, doi:10.1007/BF01061676.

Keller, O. (2009), Als der Alpenrhein sich von der Donau zum Oberrhein wandte – Zur Umlenkung eines Flusses im Eiszeitalter, in *Schriften des Vereins für Geschichte des Bodensees und seiner Umgebung*, edited by J. Klöckler, pp. 193–208, Verein für Geschichte des Bodensees und seiner, Umgebung.

Kemna, H. (2008), Pliocene and Lower Pleistocene fluvial history of the Lower Rhine Embayment, Germany: Examples of the tectonic forcing of river courses, *Quat. Int.*, *189*, doi:10.1016/j.quaint.2007.08.038.

Kock, S., J. D. Kramers, F. Preusser, and A. Wetzel (2009), Dating of late Pleistocene terrace deposits of the river Rhine using uranium series and luminescence methods: Potential and limitations, *Quat. Geochronol.*, *4*, doi:10.1016/j.quageo.2009.04.002.

Kuhlemann, J., W. Frisch, B. Székely, I. Dunkl, and M. Kázmér (2002), Post-collisional sediment budget history of the Alps: Tectonic versus climatic control, *Int. J. Earth Sci.*, *91*, doi:10.1007/s00531-002-0266-y.

Langbein, W. B., and L. B. Leopold (1964), Quasi-equilibrium states in channel morphology, *Am. J. Sci.*, *262*, 782–794, doi:10.2475/ajs.262.6.782.

Liniger, H. (1966), Das Plio-Altpleistozäne Flussnetz der Nordschweiz, *Regio Basiliensis*, *7*, 158–177.

Lucchitta, I. (1979), Late Cenozoic uplift of the southwestern Colorado plateau and adjacent lower Colorado River region, *Tectonophysics*, *61*, 63–95, doi:10.1016/0040-1951(79)90292-0.

Madritsch, H., O. Fabbri, E.-M. Hagedorn, F. Preusser, S. M. Schmid, and P. A. Ziegler (2009), Feedback between erosion and active deformation: Geomorphic constraints from the frontal Jura fold-and-thrust belt (eastern France), *Int. J. Earth Sci.*, *99*, doi:10.1007/s00531-009-0468-7.

Manz, O. (1934), Die Ur-Aare als Oberlauf und Gestalterin der pliozänen Oberen Donau, *Hohenzollerische Jahreshefte*, *1*, 113–160.

Mazurek, M., A. J. Hurford, and W. Leu (2006), Unravelling the multi-stage burial history of the Swiss Molasse Basin: Integration of apatite fission track, vitrinite reflectance and biomarker isomerisation analysis, *Basin Res.*, *18*, doi:10.1111/j.1365-2117.2006.00286.x.

Mikos, M. (1994), The Wutach gorge in SW Germany: Late Würmian (periglacial) downcutting versus Holocene processes, in *Dynamics and Geomorphology of Mountains Rivers*, edited by P. Ergenzinger, and K. H. Schmidt, 93–108, Springer, Berlin Heidelberg, doi:10.1007/BFb0117834.

Molnar, P., and P. England (1990), Late Cenozoic uplift of mountain ranges and global climate change: Chicken or egg?, *Nature*, *346*, 29–34, doi:10.1038/346029a0.

Montgomery, D. R., and W. E. Dietrich (1989), Source areas, drainage density, and channel initiation, *Water Resour. Res.*, *25*(8), 1907–1918, doi:10.1029/WR025i008p01907.

Montgomery, D. R., and K. B. Gran (2001), Downstream variations in the width of bedrock channels, *Water Resour. Res.*, *37*, 1841–1846, doi:10.1029/2000WR900393.

Morel, P., F. Von Blanckenburg, M. Schaller, P. W. Kubik, and M. Hinderer (2003), Lithology, landscape dissection and glaciation controls on catchment erosion as determined by cosmogenic nuclides in river sediment (the Wutach Gorge, Black Forest), *Terra. Nova*, *15*(6), doi:10.1046/j.1365-3121.2003.00519.x.

Müller, W. H., H. Naef, and H. R. Graf (2002), Geologische Entwicklung der Nordschweiz, Neotektonik und Lagnzeitszenarien Zürcher Wienland, Nagra. NTB, 99–08.

Muttoni, G., C. Carcano, E. Garzanti, M. Ghielmi, A. Piccin, R. Pini, S. Rogledi, and D. Sciunnach (2003), Onset of major Pleistocene glaciations in the Alps, *Geology*, *31*(11), doi:10.1130/G19445.1.

Norton, K. P., F. von Blanckenburg, F. Schlunegger, M. Schwab, and P. W. Kubik (2008), Cosmogenic nuclide-based investigation of spatial erosion and hillslope channel coupling in the transient foreland of the Swiss Alps, *Geomorphology*, *95*, doi:10.1016/j.geomorph.2007.07.013.

Paola, C., P. L. Heller, and C. L. Angevine (1992), The large-scale dynamics of grain-size variation in alluvial basins, 1: Theory, *Basin Res.*, *4*, 73–90, doi:10.1111/j.1365-2117.1992.tb00145.x.

Paola, C., and V. R. Voller (2005), A generalized Exner equation for sediment mass balance, *J. Geophys. Res.*, *110*, F04014, doi:10.1029/2004JF000274.

Petit, C., M. Campy, J. Chaline, and J. Bonvalot (1996), Major palaeohydrographic changes in Alpine foreland during the Pliocene-Pleistocene, *Boreas*, *25*, 131–143.

Peyron, O., J. Guiot, R. Cheddadi, P. Tarasov, M. Reille, J.-L. de Beaulieu, S. Bottema, and V. Andrieu (1998), Climatic reconstruction in Europe for 18,000 YR B.P. from pollen data, *Quat. Res.*, *49*, 183–196, doi:10.1006/qres.1997.1961.

Pignalosa, A., M. Zattin, M. Massironi, and W. Cavazza (2011), Thermochronological evidence for a late Pliocene climate-induced erosion rate increase in the Alps, *Int. J. Earth Sci.*, *100*, doi:10.1007/s00531-010-0510-9.

Pinter, N., R. R. van der Ploeg, P. Schweigert, and G. Hoefer (2006), Flood magnification on the river Rhine, *Hydrol. Processes*, *20*, doi:10.1002/hyp.5908.

Preusser, F. (2008), Characterisation and evolution of the River Rhine system, *Neth. J. Geosci.*, *87*.

Preusser, F., H. R. Graf, O. Keller, E. Krayss, and C. Schlüchter (2011), Quaternary glaciation history of northern Switzerland, *E&G Quat. Sci. J.*, *60*.

Prince, P. S., J. A. Spotila, and W. S. Henika (2011), Stream capture as driver of transient landscape evolution in a tectonically quiescent setting, *Geology*, *39*, doi:10.1130/G32008.1.

Raymo, M. E., and W. F. Ruddiman (1992), Tectonic forcing of late Cenozoic climate, *Nature*, *359*, 117–122, doi:10.1038/359117a0.

Rolf, C., U. Hambach, and M. Weidenfeller (2008), Rock and palaeomagnetic evidence for the Plio-Pleistocene palaeoclimatic change recorded in Upper Rhine graben sediments (Core Ludwigshafen-Parkinsel), *Neth. J. Geosci.*, *87*.

Rosenbloom, N. A., and R. S. Anderson (1994), Hillslope and channel evolution in a marine terraced landscape, Santa Cruz, California, *J. Geophys. Res.*, *99*, 14,013–14,029, doi:10.1029/94JB00048.

Schlatter, A., D. Schneider, A. Geiger, and H.-G. Kahle (2004), Recent vertical movements from precise levelling in the vicinity of the city of Basel, Switzerland, *Int. J. Earth Sci (Geol. Rundsch)*, *94*, doi:10.1007/s00531-004-0449-9.

Schlatter, A., D. Schneider, A. Geiger, and H.-G. Kahle (2005), Recent vertical movements from precise levelling in the vicinity of the city of Basel, Switzerland, *Int. J. Earth. Sci.*, *94*, 507–514, doi:10.1007/s00531-004-0449-9.

Schlunegger, F., and M. Hinderer (2003), Pleistocene/Holocene climate change, re-establishment of fluvial drainage network and increase in relief in the Swiss Alps, *Terra. Nova*, *15*(2), doi:10.1046/j.1365-3121.2003.00469.x.

Schlunegger, F., and J. Mosar (2011), The last erosional stage of the Molasse Basin and the Alps, *Int. J. Earth Sci.*, *100*, doi:10.1007/s00531-010-0607-1.

Shuster, D. L., K. M. Cuffey, J. W. Sanders, and G. Balco (2011), Thermochronometry reveals headward propagation of erosion in an Alpine landscape, *Science*, *332*, doi:10.1126/science.1198401.

Sinha, S. K., and G. Parker (1996), Causes of concavity in longitudinal profiles of rivers, *Water Resour. Res.*, *32*, 1417–1428, doi:10.1029/95WR03819.

Stock, J. D., and D. R. Montgomery (1999), Geologic constraints on bedrock river incision using the stream power law, *J. Geophys. Res.*, *104*, 4983–4993, doi:10.1029/98JB02139.

Thomas, D. S. G., and P. A. Shaw (1988), Late Cainozoic drainage evolution in the Zambezi basin: Geomorphological evidence from the Kalahari rim, *J. Afr. Earth Sci.*, *7*, 611–618, doi:10.1016/0899-5362(88)90111-X.

Törnqvist, T. E., J. Wallinga, A. S. Murray, H. de Wolf, P. Cleveringa, and W. de Gans (2000), Response of the Rhine–Meuse system (west-central Netherlands) to the last Quaternary glacio-eustatic cycles: a first assessment, *Global Planet. Change*, *27*, 89–111, doi:10.1016/S0921-8181(01)00072-8.

Ustaszewski, K., and S. M. Schmid (2006), Control of preexisting faults on geometry and kinematics in the northernmost part of the Jura fold-and-thrust belt, *Tectonics*, *25*, doi:10.1029/2005TC001915.

Vernon, A. J., P. A. van der Beek, and H. D. Sinclair (2009), Spatial correlation between long-term exhumation rates and present-day forcing parameters in the western European Alps, *Geology*, *37*, doi:10.1130/G25740A.1.

Vernon, A. J., P. A. van der Beek, H. D. Sinclair, and M. K. Rahn (2008), Increase in late Neogene denudation of the European Alps confirmed by analysis of a fission-track thermochronology database, *Earth Planet. Sci. Lett.*, *270*, doi:10.1016/j.epsl.2008.03.053.

Villinger, E. (1986), Untersuchungen zur Flussgeschichte von Aare-Donau/Alpenrhein und zur Entwicklung des Malm-Karsts in Südwestdeutschland, Jahreshefte des Geologischen Landesamtes in Baden-Württemberg, *28*, 297–362.

Villinger, E. (1998), Zur Flussgeschichte von Rhein und Donau in Südwestdeutschland, Jahresberichte und Mitteilungen des oberrheinischen geologischen, *Vereins*, *80*, 361–398.

Villinger, E. (2003), Zur Paläogeographie von Alpenrhein und oberer Donau, Zeitschrift der deutschen geologischen, *Gesellschaft*, *154*.

Wagner, G. (1929), Junge Krustenbewegungen im Landschaftsbilde Süddeutschlands. Erd- und landeskundliche Abhandlungen aus Schwaben und Franken, Vol. 10, 301 p. Öhringen.

Weidenfeller, M., and M. Knipping (2008), Correlation of Pleistocene sediments from boreholes in the Ludwigshafen area, western Heidelberg Basin, *Quat. Sci. J.*, *57*(3–4), doi:10.3285/eg.57.3-4.1.

Whipple, K. X. (2009), The influence of climate on the tectonic evolution of mountain belts, *Nat. Geosci.*, *2*, doi:10.1038/ngeo413.

Whipple, K. X., and G. E. Tucker (1999), Dynamics of the stream-power river incision model: Implications for height limits of mountain ranges, landscape response timescales, and research needs, *J. Geophys. Res.*, *104*, 17,661–17,674, doi:10.1029/1999JB900120.

Whipple, K. X., and G. E. Tucker (2002), Implications of sediment-flux-dependent river incision models for landscape evolution, *J. Geophys. Res.*, *107*(B2), doi:10.1029/2000JB000044.

Willett, S. D. (2010), Late Neogene erosion of the Alps: A climate driver?, *Annu. Rev. Earth Planet. Sci.*, *38*, 411–437, doi:10.1146/annurev-earth-040809-152543.

Willett, S. D., and F. Schlunegger (2010), The last phase of deposition in the Swiss Molasse Basin: From foredeep to negative-alpha basin, *Basin Res.*, *22*, doi:10.1111/j.1365-2117.2009.00435.x.

Wohl, E., and G. C. L. David (2008), Consistency of scaling relations among bedrock and alluvial channels, *J. Geophys. Res.*, *113*, F04013, doi:10.1029/2008JF000989.

Wong, M., and G. Parker (2006), Reanalysis and correction of bed-load relation of Meyer-Peter and Müller using their own database, *J. Hydr. Engrg.*, *132*, 1159, doi:10.1061/(ASCE)0733-9429(2006)132:11(1159).

Yanites, B. J., and G. E. Tucker (2010), Controls and limits on bedrock channel geometry, *J. Geophys. Res.*, *115*, F04019, doi:10.1029/2009JF001601.

Yanites, B. J., G. E. Tucker, K. J. Mueller, Y.-G. Chen, T. Wilcox, S.-Y. Huang, and K.-W. Shi (2010), Incision and channel morphology across active structures along the Peikang River, central Taiwan: Implications for the importance of channel width, *Geol. Soc. Am. Bull.*, *122*, doi:10.1130/B30035.1.

Zagwijn, W. H. (1989), The Netherlands during the Tertiary and the Quaternary: A case history of coastal lowland evolution, coastal lowlands, geology and geotechnology. *Proc. KNGMG symposium, The Hague*, *1987*, 107–120.

Ziegler, P. A., and M. Fraefel (2009), Response of drainage systems to Neogene evolution of the Jura fold-thrust belt and Upper Rhine Graben, *Swiss J. Geosci.*, *102*, doi:10.1007/s00015-009-1306-4.